European Journal of Pharmaceutics and Biopharmaceutics 180 (2022) 48–62

Contents lists available at ScienceDirect

European Journal of Pharmaceutics and Biopharmaceutics

journal homepage: www.elsevier.com/locate/ejpb

Research paper

Mucoadhesive brinzolamide-loaded nanofibers for alternative glaucoma treatment

Olga Cegielska [a,*], Maciej Sierakowski [b], Paweł Sajkiewicz [a], Kairi Lorenz [c], Karin Kogermann [c]

[a] Institute of Fundamental Technological Research Polish Academy of Sciences, 5B Pawińskiego St., 02-106 Warszawa, Poland
[b] Institute of Biological Sciences, Cardinal Stefan Wyszynski University in Warsaw, 1/3 Kazimierza Wóycickiego St., 01-938 Warszawa, Poland
[c] Institute of Pharmacy, University of Tartu, Nooruse 1, 50411 Tartu, Estonia

ARTICLE INFO

Keywords:
Drug delivery system
Nanofibers
Electrospinning
Cyclodextrins
Glaucoma
Mucoadhesion
Topical administration

ABSTRACT

Despite the advances in the field of pharmaceutical materials and technology, topical administration remains a method of choice for the treatment of eye diseases such as glaucoma, with eye drops being a leading dosage form. Their main disadvantage is a very short drug residence time and thus poor drug bioavailability, leading to the necessity of continuous repeated dosing. Mucoadhesive electrospun nanofibers are promising candidates for overcoming these challenges, while still benefiting from topical ocular administration. As an alternative for eye drops, a nanofibrous drug delivery system (DDS) for the delivery of brinzolamide (BRZ), based on β-cyclodextrin (β-CD), hydroxypropyl cellulose (HPC) and polycaprolactone (PCL), was designed. The results showed β-CD/BRZ guest–host interactions, successful drug incorporation into the nanofibers, and the possibility of more accurate dosing in comparison with the control eye drops. Drug permeation through sheep corneas was almost linear in time, achieving therapeutic concentrations in the receptor medium, and mucoadhesion to sheep eye mucosa was relatively high in case of formulations with high HPC content. All formulations were biocompatible, their mechanical properties were sufficient to handle them without caution and UV irradiation was suitable to reduce bioburden of the fibers matrix, yet no antibacterial properties of BRZ were observed.

1. Introduction

Glaucoma refers to a group of eye diseases leading to the optic nerve damage and consequent impairment of the visual field [1]. Associated with high intraocular pressure (IOP), it can frequently occur also at normal IOP values [2]. Brinzolamide (BRZ), the drug from the group of carbonic anhydrase inhibitors (CAIs), is particularly effective in the management of the open-angle form of a high IOP glaucoma, as it reduces the rate of aqueous humour production in the ciliary body [3]. Current treatment is made using dosage forms such as eye drops which are aqueous solutions and suspensions for topical use. Their precorneal residence time is very short, as due to reflex blinking and rapid tear turnover the drug is either eliminated from the eye surface or readily absorbed into the bloodstream through nasolacrimal duct and conjunctival vessels [4]. At the same time, anatomical diffusion barriers hinder drug permeation to interior eye tissues. As a result, the bioavailability of BRZ and other ophthalmic drugs is very low, and their stay within the therapeutic range is short, which means that immediately after administration the drug reaches a peak concentration, followed by a rapid decline [5]. To achieve the therapeutic concentration levels of drug in the eye, traditional medications have to contain an excess of the drug and be frequently administered [6]. Moreover, the topical administration of BRZ often results in ocular adverse effects such as allergic reactions, burning, stinging, general discomfort and keratitis [7]. Although at least the application of eye drops seems to be unproblematic, as eye is an easily reached external organ, medications are often installed unproperly and dosages are skipped [7]. Despite these flaws, topical therapy remains a treatment of choice for chronic ocular diseases. Systemic therapy is limited due to the blood-ocular barriers and severe systemic adverse effects [3,4]. Indeed, successful long term IOP reduction has been achieved with subconjunctivally injected suspensions of microspheres and nanoparticles [8,9], but such type of drug administration is unpleasant for patients and requires an appointment, favoring the topical use of dosage forms [10].

In recent years, several types of nanocarriers of anti-glaucoma drugs have been developed. Researchers mostly focus on nanoparticles meant to be administered in suspensions, emulsions and in-situ gelling systems [11–14]. Liquid carriers offer increased drug bioavailability, which is

* Corresponding author.
E-mail address: ocegiels@ippt.pan.pl (O. Cegielska).

https://doi.org/10.1016/j.ejpb.2022.09.008
Received 21 July 2022; Received in revised form 5 September 2022; Accepted 11 September 2022
Available online 24 September 2022

manifested by greater IOP reduction potential or similar permeability achieved with lower drug dose, yet in most cases they do not offer prolonged therapeutic effectiveness compared to control, still requiring frequent administration. This is because topical liquids, likely to locate in conjunctival sac and nasolacrimal duct, mostly omit the corneal pathway, while it is a dominating route for hydrophobic drug permeation, due to lipophilic properties of corneal epithelium. Cornea is most preferable for antiglaucoma drug administration also because it is avascular and directly linked with the ciliary body. Increasing the portion of drug permeating through cornea and minimizing the portion reaching conjunctiva and nasolacrimal duct can be achieved by solid-state carriers, adhesive to cornea enough to withstand clearance for the time of drug release. Among alternatives, such as drug-loaded inserts and contact lenses [15–19], the interest in nanofibers for antiglaucoma delivery has only recently been developed [20–22], whilst they have an enormous potential in ocular drug delivery [23]. First, they provide sustained and controlled local delivery of various active compounds, and facilitate the delivery of poorly soluble drugs [24]. They can create a stable transmembrane drug gradient that facilitates drug diffusion, resulting in increased ocular bioavailability [25]. Also, due to their large surface area, unique surface topology and porosity, they can significantly favour system's adhesion to eye mucins, which has already gained a lot of interest in pharmaceutical sciences, as it can improve the dosage residence time, therapeutic efficacy, and delivery through different routes of administration [26]. Last but not least, they can be cut in any shape and adapt to corneal surface. Nanofibers can be formed by various methods, among which electrospinning is given most attention. The process is based on electrostatic forces that elongate the polymer solution, which is accompanied by solvent evaporation, and the fibers are assembled into a nonwoven, typically on a grounded collector. It is a relatively simple and viable technique, under investigation for applications in various fields, including biomedical field [27].

It has been proven that cyclodextrins can significantly improve the corneal permeability of CAIs from solutions, in which, above different types tested, β-CD and its derivatives were found to be the most effective [28,29]. β-CD has been electrospun mostly in blends with polymers; some papers reported the possibility of obtaining pure β-CD fibers via electrospinning [30,31].

Hydroxypropyl cellulose (HPC) is a non-ionic water-soluble cellulose derivative [32]. It is approved for pharmaceutical use and used as an excipient in commercially available solutions. It has been electrospun in blends with other polymers for drug delivery and other purposes [33–35].

Polycaprolactone (PLC) belongs to a group of aliphatic polyesters. It is a hydrophobic polymer, yet biodegradable in a slow rate, and its degradation products do not cause a pro-inflammatory pH drop in the surrounding tissues. It is easily blended with other polymers and can improve the mechanical performance of a multicomponent materials, it is also easily electrospinnable using different solvent systems [36–38].

The aim of the work was to obtain a reproducible, biocompatible, mucoadhesive BRZ-loaded DDS of a high drug encapsulation efficiency, from which the drug permeates in a sustained manner. The composite polymer system was intended to be placed on cornea, to eliminate drug loss and transport via different routes than corneal. In a preferred scenario, the results would give a perspective for a sustained drug delivery, high drug bioavailability and prolonged effective therapeutic drug concentrations *in vivo*. To our best knowledge, no nanofibrous materials have been tested as BRZ carriers yet, and we hypothesised that encapsulating β-CD in the nanofibrous structure allows to fully use their potential in drug delivery.

2. Materials and methods

2.1. Materials

The following materials were used, without any further modification: PCL Mn 80,000 (Sigma-Aldrich Merck, Poland), HPC Mw 100,000 (Sigma-Aldrich Merck, Poland), β-CD (Pol-Aura, Poland), brinzolamide (BRZ; Avantor, Poland), hexafluoroisopropanol (HFIP; Iris-Biotech, Germany), Dulbecco's Modified Eagle Medium (DMEM; ThermoFisher Scientific), phosphate buffered saline pH 7.4 (1 × PBS, no calcium, no magnesium; ThermoFisher Scientific), PrestoBlue (ThermoFisher Scientific, Poland), mouse fibroblasts L929 (Sigma-Aldrich Merck, Poland), methanol (Sigma-Aldrich Merck, Poland). For permeation and mucoadhesion studies 1 × PBS pH 7.4 was prepared from tablets (Sigma-Aldrich Merck, Poland) and for the studies with the use of bacteria, Mueller Hinton broth (MHB, BD®, USA) soya-bean casein digest medium (tryptic soy broth, TSB, BD Bacto™, USA) and fluid thioglycollate medium (FTG, Lab M, UK) were prepared from powders using deionized water. For all experiments ultrapure water (Milli-Q®) was used.

Corneas were excised from sheep eyes, obtained from the local slaughterhouse according to the 3R rule (*Replacement, Reduction and Refinement*). Eight 2.9 mL glass Franz diffusion cells with spherical joints were made to order by Labit, Poland, according to author's own design.

2.2. Phase solubility of BRZ and β-CD

The phase solubility study was performed by the method reported by Higuchi and Connors [39] BRZ excess (11.5 mg) was added to increasing concentrations of β-CD in 10 mL solutions (0–13 mM), which were then magnetically stirred for 48 h at 35 °C in water baths. After this time each sample was filtered through 0.22 μm pore size syringe filter. Linear curve was fitted to datapoints corresponding to the increase in solubility of BRZ in presence of β-CD and the complexation efficiency (CE) and apparent stability constant ($K_{1:1}$) were calculated from the slope, according to Equations:

$$K_{1:1} = \frac{slope}{S_0(1 - slope)} \quad (1)$$

$$CE = S_0{}^*K_{1:1} \quad (2)$$

where S_0 is an intrinsic solubility of drug (M).

Analysis of BRZ content in the samples was performed using high performance liquid chromatography (HPLC) equipped with a UV–Vis detector (Shimadzu, Kyoto, Japan), using ARION Polar 150 mm C18 analytical column (2.2 μm; Shim-Pol, Warsaw, Poland). The mobile phase consisted of methanol and water (3:7 ratio, pH 3.7) and was pumped at a flow rate of 0.2 mL/min. The injection volume was 1 μL in all cases. The UV absorbance at 254 nm was measured.

2.3. BRZ/β-CD inclusion complexes in solid state

Inclusion complexes in solid state were prepared with equimolar ratios of BRZ and β-CD by co-evaporation and electroprocessing technique.

To obtain a co-evaporated complex, equimolar amounts of BRZ and β-CD were dissolved in HFIP (2 %w/w) in two steps. First, β-CD was dissolved in HFIP and stirred for 24 h, then BRZ was added and further stirring performed. After 24 h, the solution was left to evaporate at normal temperature and pressure conditions (NTP), followed by overnight evaporation in a vacuum oven. As a reference, pure BRZ and β-CD were subjected to the same treatment.

To obtain an electroprocessed complex, BRZ/β-CD solution of a higher total concentration (10 %w/w) was prepared the same way. Then, it was electroprocessed on a cylindrical collector using parameters established for 7.5% β-CD solution in HFIP by Kida T. *et al.*, accordingly: 25 kV voltage, 10 cm tip-collector distance, 9.6 mL/h flow rate and 250 rpm collector speed [30]. The 7.5% β-CD solution in HFIP was electroprocessed as a reference using the same parameters. Materials were then carefully removed from the collector.

BRZ/β-CD physical mixture was made by blending stock powders of these compounds in 1:1 ratio in a vial, vigorously shaking and mixing with a spatula. It was analysed immediately after preparation.

Molecular structure measurements of these two solid systems and the reference materials were performed using Fourier-transform infrared spectroscopy with attenuated total reflection sampling technique (FTIR ATR; Bruker VERTEX 70 with Platinum Diamond Micro-ATR). Measurements were performed in the range of 4000–400 cm^{-1} at 2 cm^{-1} resolution. The spectra were smoothed with 5 points and normalized, and baseline correction was applied. Smoothening did not cause any spectral changes other than noise reduction.

2.4. Electrospinning of nanofiber nonwovens

β-CD/BRZ equimolar solution was prepared in HFIP at 1.8% w/w concentration and kept under magnetic stirring for about 24 h at room temperature. Then, HPC and PCL were added in different weight ratios: 75:25, 50:50 and 25:75 (sample names: H7cd_BRZ, H5cd_BRZ and H3cd_BRZ, respectively), and kept under magnetic stirring for another 24 h. Total concentration of components in all solutions was set at 6.9 % w/w. The mass ratio of β-CD + BRZ to the polymers was set to provide 6.8% w/w BRZ in the outcome nonwoven. A negligible HPC loss in the outcome nanofibers was taken into account when estimating component ratios added to the solutions, due to HPC high electrostatic forces.

Equivalent BRZ-free solutions (H7cd, H5cd and H3cd) were prepared the same way, except BRZ was not added in the first stage of solution preparation.

For structural assessment of the nanofibers, one or more ingredient-lacking nanofiber nonwovens were also prepared: containing only PCL and HPC in three weight ratios as previously (H7, H5, H3), only HPC or PCL (HPC, PCL), HPC with β-CD (Hcd), PCL with β-CD (Pcd), HPC with β-CD and BRZ (Hcd_BRZ), PCL with β-CD and BRZ (Pcd_BRZ). All prepared formulations and their used abbreviations are provided in Table 1.

Electrospinning was performed in a horizontal mode inside an electrospinning chamber with precise temperature and humidity control (Fluidnatek® BIOINICIA, Spain). All fibers were electrospun on a negatively charged collector (-2 kV) using 13 kV voltage applied directly to the polymer solution flowing at 0.75 mL/h rate from two needles, keeping needle-collector distance approximately at 15 cm. For the preparation of all nonwovens, 40% relative humidity and 24 °C temperature were kept in the chamber during the process to ensure repeatability of the process.

Table 1
Prepared drug-loaded and non-drug-loaded nanofiber formulations; solvent – hexafluoroisopropanol (HFIP).

Formulation name	Composition	BRZ theoretical Concentration (% w/w)	β-CD Concentration (% w/w)	HPC/PCL weight ratio
Hcd_BRZ	HPC, β-CD, BRZ	6.8%	20%	–
H7cd_BRZ	HPC, PCL, β-CD, BRZ	6.8%	20%	75:25
H5cd_BRZ	HPC, PCL, β-CD, BRZ	6.8%	20%	50:50
H3cd_BRZ	HPC, PCL, β-CD, BRZ	6.8%	20%	25:75
Pcd_BRZ	PCL, β-CD, BRZ	6.8%	20%	–
Hcd	HPC, β-CD	–	21%	–
H7cd	HPC, PCL, β-CD	–	21%	75:25
H5cd	HPC, PCL, β-CD	–	21%	50:50
H3cd	HPC, PCL, β-CD	–	21%	25:75
Pcd	PCL, β-CD	–	21%	–
HPC	HPC	–	–	–
H7	HPC, PCL	–	–	75:25
H5	HPC, PCL	–	–	50:50
H3	HPC, PCL	–	–	25:75
PCL	PCL	–	–	–

Key: PCL – polycaprolactone; HPC – hydroxypropyl cellulose; BRZ – brinzolamide; β-CD – β-cyclodextrin.

2.5. Microscale morphology of the nanofibers

The morphology of the nanofibers was investigated with the use of Scanning Electron Microscope (SEM; JEOL JSM-6390LV, Tokio, Japan). For this purpose, nanofiber nonwovens were cut into small pieces and fixed on a metal microscope holder with double-sided conductive carbon tape. Prior to imaging, the samples were sputtered with about 10 nm layer of gold. The images were recorded with an acceleration voltage of 7–8 kV and a working distance of 10 mm. Magnifications of 3000x and 1500x were documented.

The fiber diameter distributions for each formulation were calculated by means of 120 measurements performed on distant locations of nonwovens using the ImageJ software. The diameter distribution was presented in the form of histograms.

2.6. Molecular structure of the nanofibers

Molecular structure measurements were performed using ATR-FTIR (Bruker VERTEX 70 with Platinum Diamond Micro-ATR). The same methodology as with complex spectra (paragraph 2.3) was used. Spectral addition of components scaled down for difference in concentrations in the fibers was analysed as a reference for the analysis of BRZ incorporation in the nanofibers.

2.7. Mechanical properties

To complement the nanofiber nonwovens characteristics, mechanical properties of the drug-loaded materials were measured in a tensile test. The test was performed using a uniaxial testing machine (Lloyd EZ-50) with a 50 N load cell under a cross-head speed of 5 mm/min, equipped with handles for thin and delicate samples. Rectangular samples of 5 × 50 mm dimensions were placed in a holder. The thickness of nonwovens was measured for each sample both sides and averaged, and included in further analysis. From the stress–strain curves, Young's modulus, tensile strength and elongation at break were determined. Each formulation was tested in 4 repetitions, on dry samples and at ambient conditions.

2.8. BRZ loading in the nanofibers

The round samples of the nanofiber nonwovens from different locations were dissolved in HFIP and vortexed for about 15 s for total dissolution. The following Equations were used for the estimation of drug loading content (DLC) and drug encapsulation efficiency (DEE):

$$DLC(\%) = \frac{mass\ of\ the\ drug\ entrapped\ in\ the\ nanofibers}{mass\ of\ the\ nanofibers} \times 100 \quad (3)$$

$$DEE(\%) = \frac{mass\ of\ the\ drug\ entrapped\ in\ the\ nanofibers}{mass\ of\ the\ drug\ added} \times 100 \quad (4)$$

As a reference, drug loading in commercial formulation Optilamid® (1 mg/mL BRZ) was also tested. For this purpose, one drop of formulation was suspended in deionized water and vortexed to obtain a solution. Each formulation was tested in triplicate. The samples were diluted 5 times and analysed for drug content by HPLC according to the method described in paragraph 2.2.

2.9. Mucoadhesion of the nanofibers

Mucoadhesion of the drug-loaded nonwovens was tested using CTX texture analyser with 1 kg load cell (AMETEK Brookfield, Middleborough, MA, United States, purchased via Labo Plus, Warsaw, Poland; Fig. 1). The round samples of drug-loaded nonwovens (H7cd_BRZ, H5cd_BRZ, H3cd_BRZ) with the diameter of 10 mm were attached to the 10 mm diameter 35 mm long cylinder probe with a double-sided adhesive tape. Freshly excised sheep eyeballs were fixed in a custom holder and either left with their natural moisture or wetted with PBS (pH 7.4) to mimic lachrymation by pipetting PBS until entire cornea was covered. First, the probe was lowered with 1 mm/s speed to enable contact of the nonwoven with cornea until 0.1 N was achieved, and after 10 s of contact with 0.1 N it was moved upwards at the speed of 1 mm/s to separate the sample from the cornea. For each measurement, a fresh cornea was used. Mucoadhesion was characterized by maximum force and total work required to detach the nonwoven from the cornea. Work of mucoadhesion was calculated by measuring the area under force vs distance curve. Force of detachment was defined as a peak force able to detach the nonwoven from the cornea. The test was filmed to give an insight in the process. Each formulation was tested in 4 repetitions per conditions (dry/wet).

2.10. Release of BRZ from the nanofibers and permeation through sheep corneas ex vivo

The study of BRZ release and permeation *ex vivo* was performed in 2.9 mL Franz diffusion cells with spherical joints (Fig. 2). Sheep was chosen as an animal model due to anatomical and clinical characteristics of the eyeball, making it more suitable for drug delivery studies than small laboratory animals [40]. Freshly excised sheep corneas rinsed with PBS (pH 7.4) were mounted separately on spherical joints of the acceptor chambers. Acceptor chambers were filled with PBS and previously weighted round nanofibrous samples with the diameter of 10 mm (3.5–4 mg) or a drop of commercial eye drop formulation as control (Optilamid®) both containing similar BRZ amount, according to own data and manufacturer's declaration, were placed centrally on the corneas. The donor chambers were placed on the acceptor chambers and each pair was connected with metal clamps and sealed with paraffin foil (Parafilm®) on the top to avoid fluid evaporation and maintain continuous moisture of the corneas. The cells were then put in water baths and placed on magnetic stirrers maintaining constant stirring and heat in order to maintain 35 °C in water baths, to mimic ocular surface temperature of glaucomatous eyes [41]. At six predetermined intervals, samples of 400 µL each were collected through the sampling ports by 2 mm wide, 120 mm long stainless-steel needles. After each sampling the acceptor chambers were topped up with 400 µL of PBS through the sampling ports. Each formulation was tested in at least 13 repetitions. The samples were analysed for drug content by HPLC according to the method described in paragraph 2.2. Results were converted to cumulative permeated BRZ amount per sphere diffusion area (µg/cm^2), averaged and plotted as a function of time (h) with 95% confidence limits. Steady state flux (Jss) and lag time for each formulation, including control, were calculated from the linear functions obtained in a linear regression model. The small volume of a Franz cell donor compartment most closely mimicked *in vivo* fluxes, yet lacrimation or eyelid motion were neglected, in accordance with the generally accepted methodology.

2.11. UV treatment

For biocompatibility study and bacterial studies, the materials were cut in appropriate pieces and disinfected with ultraviolet (UV) light under the laminar hood for 1 h, 30 min per sample side.

2.12. In vitro biocompatibility of the nanofiber nonwovens

2.12.1. Cell culture

L929 mouse fibroblasts were cultured in Dulbecco's minimum essential medium (DMEM), 10% Fetal Bovine Serum (FBS) and 1% antibiotic (penicillin/streptomycin). The details are given in the Supplementary Materials.

2.12.2. Cytotoxicity

In order to determine cellular response to the nanofibers, the test of cytotoxicity of material extracts on mouse fibroblasts L929 was performed by cell metabolic activity testing with PrestoBlue assay, where mitochondrial metabolic activity of the cells is measured.

For this purpose, UV-treated 5 mm diameter round samples of drug-loaded and corresponding non-loaded nanofiber nonwovens were placed in the wells of three 96-well plates in 6 repetitions, and 200 µL of culture medium was added to the wells to make material extracts. Pure culture medium served as a negative control. The plates were then incubated at 37 °C in an orbital shaker maintaining mild stirring.

At the same time L929 cell suspension was seeded into another three 96-well plates at the density of 3000 cells per well. The plates were then incubated at 37 °C and 5% CO_2.

After 24 h, the culture medium from cell-seeded wells was replaced

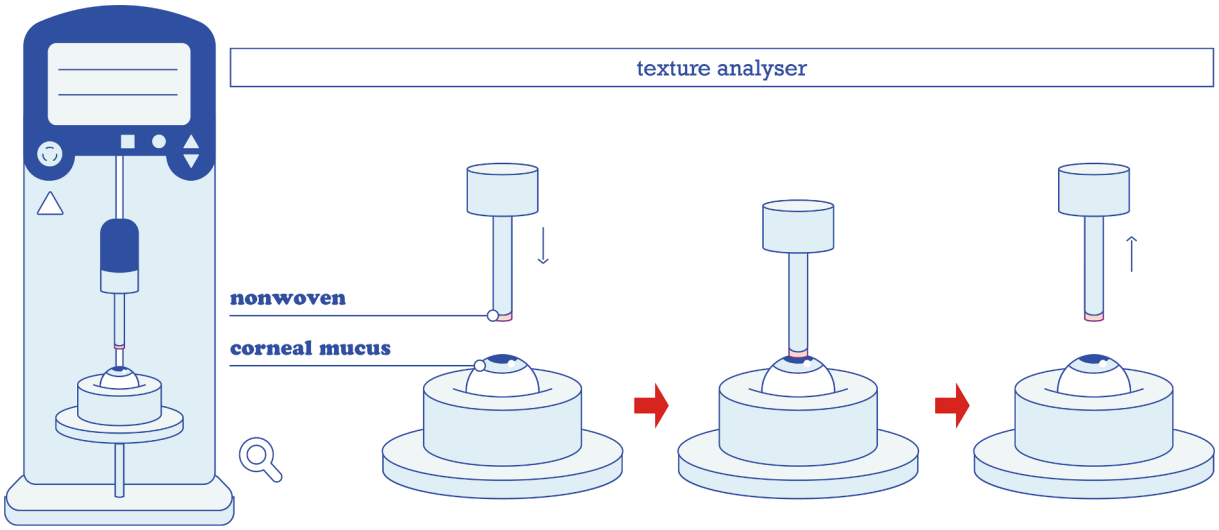

Fig. 1. Illustration of the experimental setup for mucoadhesion study on cornea.

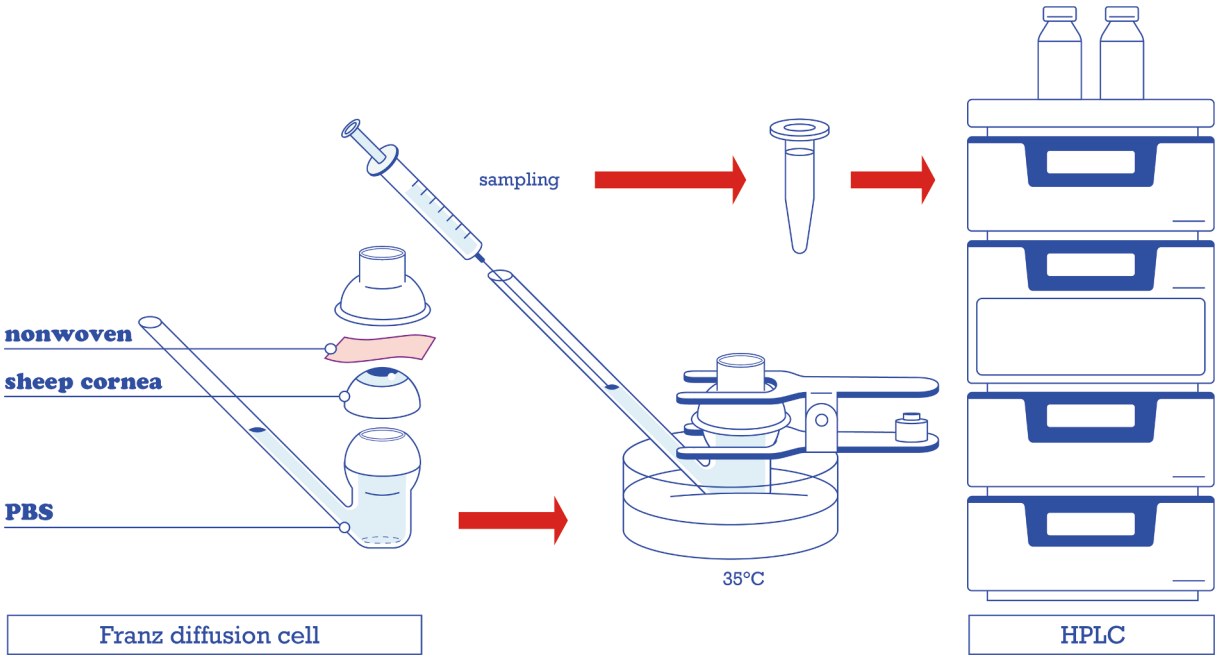

Fig. 2. Illustration of the experimental setup designed to test permeation of brinzolamide (BRZ) from nanofibers through sheep corneas.

with material extracts, except one row per plate that served as a positive control (cells in growth medium), and the plates were incubated at 37 °C and 5% CO_2 for another 24, 48 and 72 h (one plate per time point).

After specified time-periods, the cell metabolic activity test was performed according to PrestoBlue assay. For this purpose, all fluids were replaced with 200 μL of Presto Blue solution (1 %v/v PBS). The plates were then vigorously shaken with a vortex and incubated at 37 °C and 5% CO_2 for 40 min. After this time, solution samples from each well were transferred to a new 96-well plate, and the fluorescence was measured using fluorometer with excitation at 530 and emission at 620 nm (Fluoroskan Ascent TM Microplate Fluorometer, Thermo Scientific, USA). Corrected fluorescence was calculated by subtracting the average control well value from that of each experimental well. The results were presented as mean fluorescence units with 95% confidence limits.

2.13. Bacterial studies

2.13.1. Bacterial cultures

P. aeruginosa (DSM no.: 1117) *and S. aureus* (DSM 2569), obtained from the Leibniz Institute DSMZ-German Collection of Microorganisms and Cell Cultures, were cultured on lysogeny broth (LB) agar from DMSO stocks. The details of bacterial culture method and preparation of DMSO stocks are given in the Supplementary Materials.

2.13.2. Sterility

Sterility test of the samples was performed according to the European Pharmacopoeia (9.0) in tryptic soy broth (TSB) and thioglycollate media (FTG). The media were prepared from powders according to the manufacturer's instructions, poured into glass tubes in 5 mL volume, and autoclaved. After the media had cooled down to room temperature, square 1 × 1 cm samples of UV-treated and untreated non-drug-loaded nanofiber nonwovens were put inside the tubes under aseptic conditions, in triplicates. TSB and FTG media, inoculated with *S. aureus* and *P. aeruginosa*, respectively, served as positive controls, and pure growth media served as negative controls. Tubes with FTG were incubated in anaerobic conditions at 30 °C and tubes with TSB in aerobic conditions at room temperature (20–25 °C) for 14 days. The tubes were visually evaluated for any presence of microorganism growth and photographs were taken. The sample complied with the test for sterility if no microbial growth was found after the incubation period of 14 days in any of the replicates. For the test to be valid, no growth can occur in negative controls, whereas in positive controls the growth must occur.

2.13.3. Minimum inhibitory concentration

Minimum inhibitory concentration (MIC) of BRZ in the concentration range of 11.25–0.022 mg/mL against *S. aureus* and *P. aeruginosa* was tested using broth microdilution method [42]. BRZ solution was prepared in HFIP/water (1:1) to increase BRZ solubility, and further diluted with distilled water 8 times. Prior to testing, the MIC test with pure solvent system was performed, in which 3.125% concentration of HFIP was established as a maximum nonharmful concentration to *P. aeruginosa* – and none of the tested concentrations were found harmful to *S. aureus*.

Overnight liquid culture of bacteria in LB broth was serially diluted to about 10^3 colony-forming units (CFU)/mL with Mueller Hinton broth (MHB) and plated out (5 μL drops) on LB agar plates as bacterial controls. Erythromycin 0.64 mg/mL and tetracycline 1 mg/mL aqueous solutions were prepared as antibiotic controls for *S. aureus* and *P. aeruginosa*, respectively. Pure broth served as negative controls and bacterial suspensions served as positive controls. To establish the MIC value, visual turbidity in the wells was evaluated after overnight incubation at 37 °C and the photographs were taken. The test was performed separately for each bacterium.

The test methodology was also used to evaluate the growth inhibition potential of the BRZ-loaded HPC/PCL/β-CD nonwovens consisting BRZ in concentrations used in the standard MIC test, determined by the weight of the samples. For this purpose, 6 mm diameter round UV-treated drug-loaded and non-loaded nonwoven samples were individually placed into the broth-filled wells in triplicates, prior to adding bacterial suspensions. Antibiotic dilutions, positive and negative controls were made as previously described. To establish if nonwovens caused the inhibition of bacterial growth, visual turbidity in the wells was evaluated after overnight incubation.

2.14. Statistical and data analysis

All experiments were performed in repetitions, as specified in the

methodology section.

General linear model (GLM) class was used in the analysis. The models used for the test variables were selected from the GLM class using The Akaike information criterion (AIC). In the case of repeated measurements along the time factor, the covariance matrix of the random component was adjusted. The comparisons of mean values were performed using Tukey's HSD tests (Honestly Significant Differences).

A Shewhart XR Control Chart was used to compare the drug content in the formulations. The model assumes that changes within the control limits are due to random causes.

The p value of < 0.05 was considered as statistically significant. The calculations were processed in SAS/STAT rel. 15.2 (SAS analytics, Poland).

Data are presented as an arithmetic mean with standard deviation (SD) or least squares (LS) mean with 95% confidence limits.

3. Results and discussion

3.1. β-CD/BRZ interactions in solid-state

Electroprocessing of β-CD solution in HFIP resulted in the formation of ribbon-like fibers with beads, whereas electroprocessing of BRZ/β-CD solution led to the formation of irregular locally elongated clusters (Fig. 3 a-b). Both materials were very brittle, which were easily breaking when handled.

FTIR analysis was performed in order to verify the formation of inclusion complex of BRZ and β-CD, as secondary interactions between components can be detected by shifts in wavelength. The complex

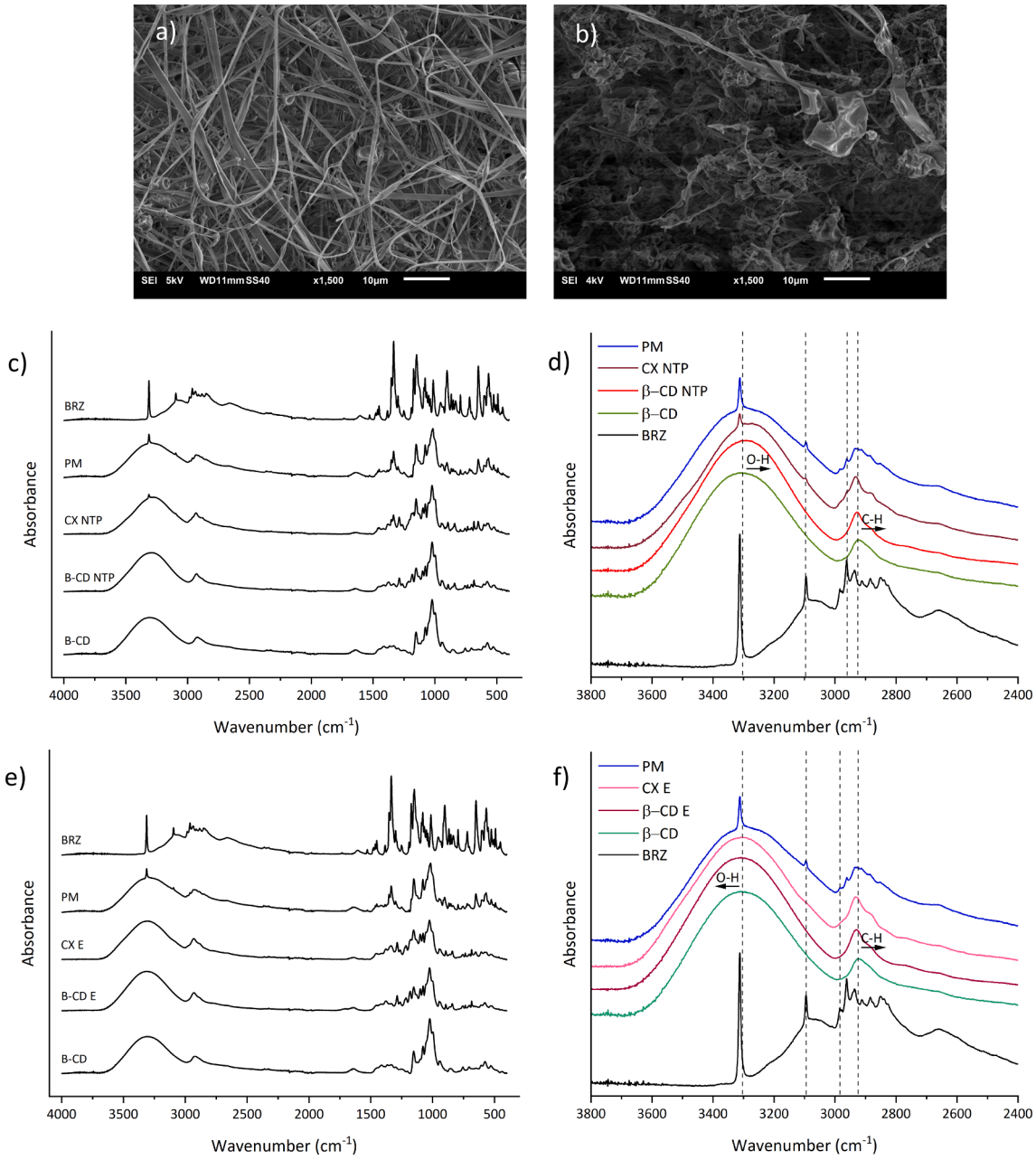

Fig. 3. SEM images of β-CD (a) and BRZ/β-CD (b) structures formed by solution electroprocessing; (c-f) FTIR spectra of solid-state β-CD/BRZ complexes and reference materials with a close-up on 3800–2400 cm^{-1} regions (d, f); important peaks including hydroxyl (OH–) and CH band are marked, with a graphical presentation of the direction of wavenumber changes (d, f). Keys: BRZ – brinzolamide; PM – β-CD/BRZ physical mixture; CX NTP – β-CD/BRZ co-evaporated complex; CX E - β-CD/BRZ electroprocessed complex; β-CD NTP – β-CD co-evaporated, β-CD E – β-CD electroprocessed; β-CD – β-CD powder.

spectra were compared with the spectra of pure compounds and their respective physical mixture.

The spectrum of pure BRZ powder showed typical bands of the compound: a sharp peak at 3312 cm^{-1}, assigned to N-H stretching in the primary amine group; at 2962 cm^{-1}, assigned to CH_3 stretching, and at 2853 and 1451 cm^{-1}, assigned to $–CH_2$ stretching; multiple peaks in the range of 1400–1300 cm^{-1} and 1200–1100 cm^{-1}, assigned to double asymmetric and symmetric S = O stretching in two sulfonyl groups, respectively; and at 649 and 3095 cm^{-1}, attributed to heterocycle containing S and N elements [43] (Fig. 3 c-f). The spectra of BRZ powder and evaporated BRZ were identical, proving that no degradation nor solid state changes of BRZ occurred in the solution or during drying.

The pristine β-CD powder spectrum was also in accordance with the literature data. A broad band in the range of 3000–3600 cm^{-1} could be assigned to OH groups vibrations and comprised of overlapping subbands of primary and secondary OH groups. The peak at 2924 cm^{-1} was assigned to C–H asymmetric/symmetric stretching; at 1645 cm^{-1} to H–O–H deformations; at 1153 and 1023 cm^{-1} to C–H overtone stretching and at 1029 cm^{-1} to C–H, C–O stretching [44] (Fig. 3 c-f).

Electroprocessed and evaporated β-CD spectra were almost identical, differing only slightly in the intensities of individual bands, yet differing from raw β-CD powder spectrum. No peaks disappeared in the HFIP-treated systems, but several new ones appeared: at 685, 840, 894 and 1263 cm^{-1} and the peak at 1100 cm^{-1} became more intense. While alterations of already existing peaks could be due to minor bond changes during recrystallisation [45] it is possible that the new ones originated from HFIP residues, as CF group can be found at 894 and 1263 cm^{-1} and CF_3 group at 1100 cm^{-1} [46,47]. HFIP incorporation within β-CD cavity is in accordance with the data described by Kida *et al.* [30]. There was also a shift of O–H and C–H band in both spectra (Table 2) and in the electroprocessed spectrum a hump appeared at about 1711 cm^{-1} (Fig. 3 c-f).

BRZ/β-CD physical mixture spectrum was approximately the superposition of BRZ and β-CD spectra. The OH band position changed due to the superposition of BRZ and β-CD spectra, which shifted the OH band towards lower wavenumbers (Fig. 3 c-f).

The electroprocessed complex spectrum of BRZ-β-CD was almost identical to the electroprocessed β-CD spectrum, same as the co-evaporated complex spectrum was almost identical to the evaporated β-CD spectrum. The absolute shifts were equal or higher than in the HFIP-treated β-CD spectrum, including positive and negative shifts (Table 2). The OH band shifted slightly in the electroprocessed complex spectrum and significantly in the co-evaporated complex spectrum, yet the symmetry of the peak tip did not change, contrary to what was visible in the physical-mixture spectrum. It also became narrower in the co-evaporated complex spectrum. Most of BRZ peaks were absent or relatively low in intensity compared to BRZ and physical mixture spectral peaks, including BRZ N–H peak at 3312 cm^{-1}, which was reduced in the co-eveporated complex spectrum and disappeared completely in the electroprocessed complex. It could be indicative of the involvement of BRZ's N–H group in complexation with CD. Finally, a hump that appeared at about 1711 cm^{-1} on the side of the peak in the spectrum of electroprocessed β-CD was no longer present in the spectrum of electroprocessed complex (Fig. 3 c-f).

Frequency shifts, broadening and disappearing of the drug's characteristic bands, as well as changes in their shape compared to those recorded in the spectra of pure BRZ and a physical mixture of BRZ and β-CD, are considered to evidence a modification of bond strengths and lengths, being a consequence of host–guest interactions upon complexation. Also narrowing of the β-CD OH band, that has been observed by many researchers, is considered to indicate the formation of an inclusion complex [48,49]. Therefore, the host–guest complex formation between BRZ and β-CD in solid state was confirmed. What it may also show, are the dynamical properties of β-CD in solution and the driving force of complex formation – when BRZ hydrophobic molecules become present in the system, they readily replace solvent's polar molecules, leaving the spectra almost unchanged compared to those of pure HFIP-treated β-CD [50].

Table 2
Positions of the OH and CH stretching bands of analysed compounds (cm^{-1}).

Sample	β-CD	β-CD E	CX E	β-CD RT	CX RT
OH–	3304	3307	3306	3293	3282
CH–	2924	2930	2933	2927	2933

Keys: CX – complex, β-CD – β-cyclodextrin, NTP – evaporated/co-evaporated, E – electroprocessed.

3.2. β-CD/BRZ interactions in solution

Phase solubility diagram showed that β-CD significantly increased BRZ solubility in PBS, which confirmed guest–host interactions between these components (Fig. 4). β-CD at 7 mM concentration enabled the dissolution of all BRZ present in the system, and above that concentration BRZ solubility decreased down below its solubility limit. Such course of the curve classifies it to the B phase type, according to standard classification introduced by Higuchi and Connors [39], characteristic to complexes with limited water solubility, and common for systems with β-CD. No plateau phase between increase and decrease in solubility was observed due to depletion of the drug. The drop in drug solubility is explained by the formation of precipitating complex after all of the solid drug was dissolved during complexation [51]. Macroscopic visual observation of the solutions complements this statement, as they were cloudy and full of precipitate.

BRZ is a hydrophobic drug that has the maximum tendency to partition from the tear fluid into cornea in physiological pH, yet becomes soluble only in acidic conditions [52]. In marketed eye drops pH-modifiers such as HCl or NaOH are used to improve its solubility [53]. β-CD, hydrophilic at the outer surface and hydrophobic in the cavity, increase drugs' solubility not by pH adjustment, but by forming a guest–host complex by means of intermolecular hydrogen bonds, where the drug is a guest molecule [54]. The drug is then dissociated from the cavity either through complex dilution in the aqueous tear fluid or direct partition into the lipophilic epithelium [55]. Complexes of B-type characteristics allow to enhance drug permeation through cornea very effectively by keeping an excess of the drug dissolved in aqueous solution thanks to dissolved CD-s, while the rest of them forms a stable slowly releasing drug reservoir in the preocular space. The chemical potential, which drives the passive diffusion through mucous layer and eye membranes, is then at its maximum [29].

Compared to other CD-s that have been tested in systems with BRZ, β-CD was much more successful in improving BRZ solubility, achieving

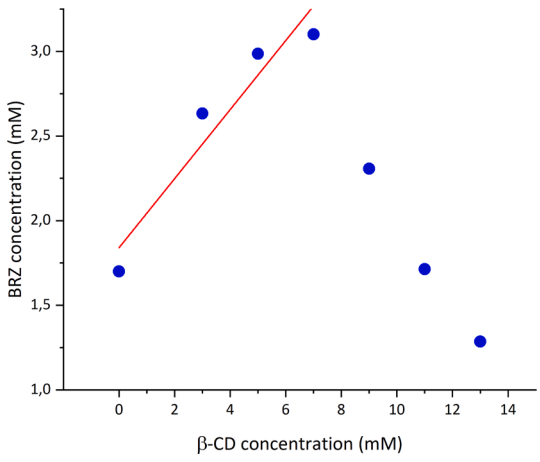

Fig. 4. Phase solubility diagram of brinzolamide (BRZ) in the presence of increasing concentration of β-cyclodextrin (β-CD) in PBS at 35 °C.

higher CE and $K_{1:1}$ values – 0.26 and 151 M^{-1}, respectively [28]. 1:1 M ratio of β-CD and BRZ was chosen for incorporation into the nanofibers, as due to BRZ release from the fibers, its amount would slowly decrease in relation to β-CD (Fig. 4, pointing towards right side on the graph).

3.3. Nanofibers formation and characterisation

The electrospinning of the drug-loaded solutions was successful. Slight jet instability, as well as fiber attraction outside a collector, was observed during electrospinning solutions containing HPC in majority, but it didn't have a negative impact on fibers morphology. As anticipated, all BRZ-loaded nanofibers were similar, they had a smooth texture and were randomly distributed in the nonwoven (Fig. 5). Fiber diameter distribution of all materials was bimodal, very similar for H5cd_BRZ and H3cd_BRZ formulations, with similar median values, and different for H7cd_BRZ, with lower median values. Fiber diameters ranged from several dozen nanometres to about 1 μm, placing them in nano and micro-scale (Fig. 5). Description of the electrospinning process and morphology of the drug-free nanofibers together with SEM images can be found in the Supplementary Materials (Fig. A.1).

3.4. Structural analysis

The FTIR spectra of nanofibers were analysed to acknowledge possible interactions between their components. They were carefully compared with the spectra of neat nanofibers, multicomponent nanofibers lacking each one ingredient and spectral additions of components.

FTIR spectrum of pristine PCL nanofibers showed typical bands of the polymer: at 2865 cm^{-1} and 2944 cm^{-1}, corresponding to the symmetric and asymmetric CH_2 stretching vibrations, respectively; at 1723 cm^{-1}, related to the C=O stretching vibration; at 1294 cm^{-1}, assigned to the C–C and C–O stretching modes in the crystalline PCL; and at 1165 cm^{-1} and 1240 cm^{-1}, assigned to symmetric and asymmetric C–O–C stretching vibrations, respectively (Fig. 6a) [56]. The carbonyl band consisted of two sub-bands attributed to crystalline and amorphous regions, evidenced by a hump on a peak shoulder [57].

In the FTIR spectrum of pristine HPC nanofibers there was a broad band with maximum at about 3436 cm^{-1} coming from hydroxyl group. There were slight differences in other bands shape, relative intensities and positions compared to the literature data (collected for weathered HPC or tested with KBr method), yet most of them were identified in the sample: at 2969 and 2873 cm^{-1} assigned to C–H asymmetric and symmetric vibrations; at 1052, 1079 and 1119 cm^{-1} assigned to C–O stretching vibrations, at 1453 cm^{-1} probably assigned to O–H, C–H bending and $–CH_2$ deformation; and at 1374 and 1325 cm^{-1} to $–CH_2$ wagging and C–H and O–H bending vibrations (Fig. 6a) [58]. To ensure solvent treatment and electrospinning did not change the structure of the polymer, substrate in powder form was tested spectroscopically as a reference to the nanofibers. The spectra were identical.

The spectra of two-component nanofibers – H7, H5, H3, Hcd, Pcd (Table 1) – were a result of overlapping individual bands of their components with no visible alterations.

In the spectra of PCL-containing materials, the position of carbonyl stretching band varied, most probably due to differences in the fraction of amorphous and crystalline regions in PCL, shifting the maximum absorbance peak and causing humps on its side. In general, in most cases with each component added to the system, the peak shifted toward higher wavenumbers, proving increase in amorphous fraction, except when it was still a predominant ingredient (Table 3, Fig. 6b).

In the spectrum of Hcd_BRZ and Pcd_BRZ, BRZ peaks were mostly absent or had a very low intensity. Only approximately at 607 and 1325 cm^{-1} there were evidences of BRZ vibrations, in case of HPC overlapping with its peaks and increasing their intensity. In both materials the peak at 649 cm^{-1} moved towards higher wavenumbers (652 cm^{-1}), indicating that the S–N heterocycle of BRZ was engaged in forming bonds with some of the two other components. Also, OH band shifted compared to BRZ-lacking materials toward lower wavenumbers, in case of Hcd_BRZ from approximately 3401 to 3398 cm^{-1}, and

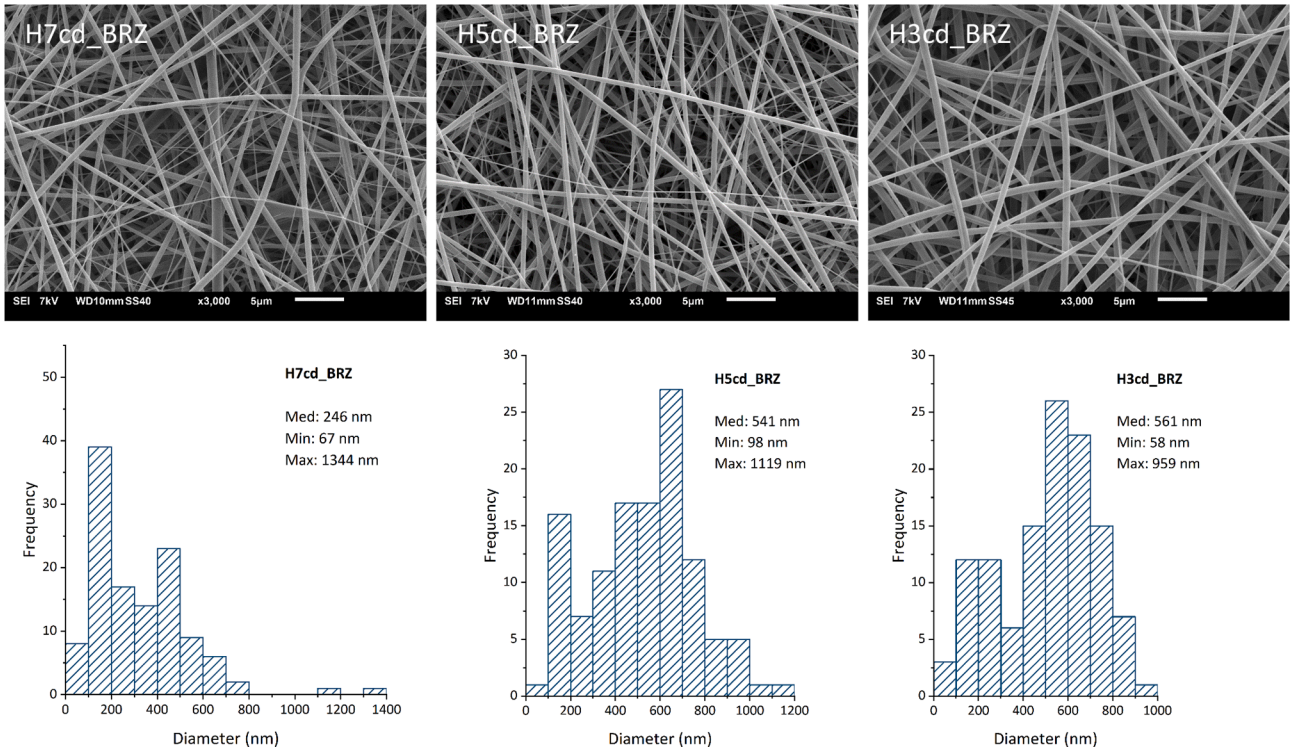

Fig. 5. SEM images of the brinzolamide (BRZ)-loaded nanofibers (H7cd_BRZ, H5cd_BRZ, H3cd_BRZ) and histograms presenting diameter distribution of these fibers in the nanofiber nonwovens (n = 120). Keys: Med – median, min – minimum, max – maximum [fiber diameter]. Reference is made to Table 1 for different formulations.

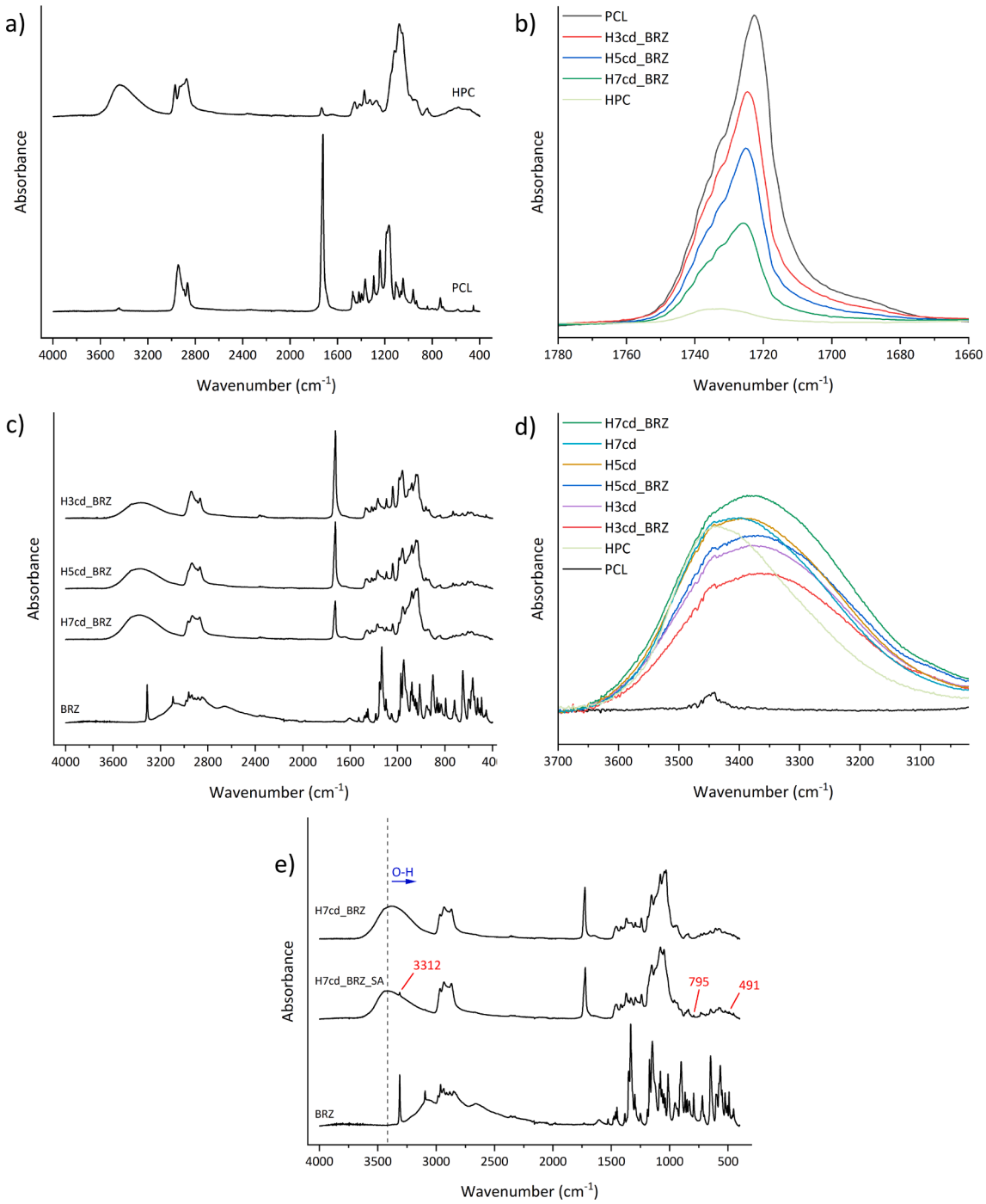

Fig. 6. FTIR spectra of the non-drug-loaded reference nanofibers (a) and BRZ-loaded nanofibers (b-e), including: close-up view on carbonyl band (in the region of 1780–1660 cm^{-1}) (b) and hydroxyl band (in the region of 3700–3000 cm^{-1}) (d) of nanofibers spectra; comparison of H7cd_BRZ material spectrum to spectral addition of its components scaled down to account for difference in concentrations in the nanofibers (e); BRZ peaks present only in spectral addition and OH shift direction are marked. Keys: HPC – hydroxypropyl cellulose; PCL – polycaprolactone; β-CD - β-cyclodextrin; BRZ – brinzolamide; H7cd_BRZ – HPC with PCL in 75:25 ratio with β-CD and BRZ; H7cd - HPC with PCL in 75:25 ratio with β-CD; H5cd_BRZ – HPC with PCL in 1:1 ratio with β-CD and BRZ; H5cd - HPC with PCL in 1:1 ratio with β-CD; H3cd_BRZ - HPC with PCL in 25:75 ratio with β-CD and BRZ; H3cd - HPC with PCL in 25:75 ratio with β-CD; H7cd_BRZ_SA – spectral addition of components of H7cd_BRZ material. Reference is made to Table 1 for different formulations.

Table 3
Positions of the carbonyl (CO–) stretching band of analysed fibers (cm^{-1}). Reference is made to Table 1 for different formulations.

Sample	PCL	PCLcd	PCLcd_BRZ	H7	H7cd	H7cd_BRZ	H5	H5cd	H5cd_BRZ	H3	H3cd	H3cd_BRZ
C = O	1723	1722	1723	1725	1725	1726	1724	1725	1725	1723	1723	1725

Pcd_BRZ from approximately 3362 to 3348 cm^{-1}, yet its symmetry did not change, most likely evidencing BRZ interaction with CD specifically.

The spectra of BRZ-loaded multicomponent nanofibers were almost identical as corresponding drug-free nanofibers spectra. The same BRZ evidences and shifts as in the Hcd_BRZ and Pcd_BRZ spectra were found, including the shift of S–N heterocycle peak from 649 to 652 cm^{-1}, and a barely noticeable hump at 3095 cm^{-1}, assigned to BRZ S–N heterocycle. Whilst in the spectral addition of components BRZ peaks at 491, 795, 3095 and 3312 cm^{-1} were clearly visible, they were all absent in all drug-loaded fibers spectra (Fig. 6e). This points to drug and β-CD being present in the nanofibers in the form of complex (Fig. 6c).

In all multicomponent nanofiber's spectra, the OH band position varied due to superposition of OH bands coming from different components in this area, but a trend could be noticed for drug-loaded samples spectra, where it was shifted toward lower wavelengths, compared to analogous drug-free samples and the spectral additions, and the shifts were higher the more HPC was present in the sample (Fig. 6d). The shift of OH band was already recognized in Hcd_BRZ spectrum. We anticipate that these shifts origin in β-CD and BRZ guest–host interactions, favoured by HPC, possibly remaining close to each other in the structure.

To conclude, PCL present in the fibers was semi-crystalline and each component present in the system hindered its crystallization. No straightforward evidences on interactions between polymers as well as polymers with β-CD alone were found in the spectra, yet BRZ was definitely linked with other fiber components, among others by S–N heterocycle and N–H in the primary amine group, CH_3 and $–CH_2$, which bands were absent or shifted in the spectra (positions 3095 and 649, and 3312 cm^{-1}, respectively). It is most probable that it was complexed by β-CD, as shown by OH group shifts in the presence of HPC, which favoured the complexation. No peaks that could evidence residues of HFIP were present in any spectra, proving effective solvent evaporation from the thin fibers during electrospinning.

3.5. Mechanical strength

The mechanical properties of biomaterials intended for ocular administration are important for their handling and durability. External ocular inserts, including DDs, are generally exposed to mild stress generated by blinking action of the eye and handling. Typically, tensile strength and elongation at break are used to evaluate their mechanical performance [59–63].

In the stress/strain curves of BRZ-loaded materials containing HPC predominating over PCL (H5cd_BRZ and H7cd_BRZ) two stages were distinguished – a linear elastic Hookean response and a non-linear plastic behaviour finished with a specimen rupture. In the curves of H3cd_BRZ material, another stage was observed after a linear response and prior to the rupture, evidenced by more than one decline in stress, alternating with the elongation of unperturbed regions. This stage corresponded to the formation of multiple localized necks in the specimens, and was the reason of break which appeared long after achieving the tensile strength. The elongation at break value of H3cd_BRZ nonwoven was much higher and statistically different from other values characterizing two other nonwovens (H5cd_BRZ and H7cd_BRZ). The tensile strength was also much higher. In turn, Young's moduli of the BRZ-loaded nonwovens with PCL predominating over HPC (H5cd_BRZ and H3cd_BRZ) were almost equal, while Young's modulus of nonwovens consisting mostly of HPC (H7cd_BRZ) was higher and differed statistically (Table 4).

Necking is not a characteristic feature of nanofibrous nonwovens nor PCL materials, and it generally indicates the occurrence of local instabilities in the specimen. Multiple necking was reported only in polymer materials containing organized porous microstructure and nanofibers. While in the formers it can be easily explained by alternating microcracks and elongation in the lattice, in the latter it is rather explained by an exceptional possibility of the nanofibers to accommodate many perturbation wavelengths, and thus more than a single neck, due to much higher length to diameter ratios than those of macroscopic polymer materials [64,65]. The second explanation however is not universal, as not often multiple necking is observed in nonwovens made on nanofibers. The reason behind such mechanical behaviour of H3cd_BRZ only could have been the weakest bonding between the components in comparison with other two formulations (Fig. 6 and Table 3). The material might have repeatedly broke in brittle regions and elongate in elastic PCL regions, rather pointing to the importance of chemical variability within the specimen. Because H3cd_BRZ sample was dominated by PCL, its time to rupture was relatively high compared to two other nanofiber nonwovens (H5cd_BRZ and H7cd_BRZ), in which high percentage of brittle components, HPC, β-CD and BRZ, and higher interactions between components, didn't allow even local elongation.

What is important from the point of user, the mechanical parameters of the proposed DDs were sufficient to withstand stress applied with hands without tearing, providing unproblematic handling and usage. Both tensile strength and elongation of H7cd_BRZ and H5cd_BRZ formulations were in between the values reported for other developed materials for ocular application, and similar values of elongation induced by much lower values of tensile stress were considered satisfying for handling and storage of the bioadhesive ocular insert with aceclofenac [59–63].

3.6. Drug loading

The drug loading in the nanofibers was similar to the expected value (6.8% w/w in solid state) in all formulations (Table 5). There were small deviations among loading content values of each formulations and locally the encapsulation efficiency exceeded 100%, suggesting slight unevenness in drug distribution among the nanofiber nonwovens, but no drug loss during the electrospinning of nanofibers. There were also no statistical differences in drug distribution between the same formulation samples from different batches, proving reproducible electrospinning of the nanofibers.

High encapsulation efficiency is highly desirable in drug carriers, as it prevents wastage of drug. Process repeatability, in turn, is essential when considering translating the carrier production from laboratory to a commercial scale.

The commercial formulation was found to contain different amounts of BRZ per drop due to the different volume of the drop squeezed from the dispenser (Table 6). Therefore, the nonwovens with a given drug distribution, give also an opportunity to tailor a more precise drug dosing by cutting a piece of nonwoven of an appropriate weight.

Table 4
Average Young modulus, elongation at break and tensile strength values of the brinzolamide (BRZ)-loaded nanofiber nonwovens. Data are expressed as a mean ± standard deviation.

Formulation	Young modulus	Elongation at break (%)	Tensile strength (MPa)
H7cd_BRZ	112.75 ± 25.04	9.69 ± 1.11	5.9 ± 0.54
H5cd_BRZ	89.52 ± 4.25	8.77 ± 1.43	4.36 ± 0.45
H3cd_BRZ	90.86 ± 6.24	211.05 ± 80.06	8.21 ± 0.44

Table 5
Drug (BRZ) loading content and drug encapsulation efficiency in the electrospun nanofiber nonwovens from two different batches. Data are expressed as a mean ± standard deviation (n = 3).

Formulation	Loading content ± SD (%)		Encapsulation efficiency ± SD (%)	
	Batch 1	*Batch 2*	*Batch 1*	*Batch 2*
H7cd_BRZ	6.46 ± 0.24	6.53 ± 0.43	95.07 ± 3.56	95.98 ± 6.35
H5cd_BRZ	6.69 ± 0.23	6.83 ± 0.13	98.36 ± 3.34	100.40 ± 1.87
H3cd_BRZ	7.38 ± 0.48	7.07 ± 0.23	108.48 ± 7.05	103.93 ± 3.44

Table 6
Drug (BRZ) amount in one drop of commercial formulation Optilamid®. Data are expressed as a mean ± standard deviation (n = 3).

Formulation	Measured drug amount ± SD (μg)	Theoretical Drug amount (μg)
Optilamid®	234.17 ± 48.47	270

3.7. Mucoadhesion

The values of force of mucoadhesion and work of detachment, named force and work of mucoadhesion, increased with HPC content in the nanofiber nonwovens both in non-wetted and wetted conditions (named dry and wet) and the differences were statistically significant when analysed independently in these test conditions (dry/wet). When wetting was the only variable, both work and force were also statistically lower in wet conditions. When both variables (test conditions and formulation compositions) were taken into the analysis, average force and work values decreased inversely proportional to HPC amount in the nonwovens, however, when comparing two adjacent formulations, wetting often decreased the mucoadhesion of that with the higher HPC amount to a level characterising that with the lower HPC amount in dry conditions. Still, both force and work of detachment of H7_BRZ in dry conditions were superior in comparison to H5_BRZ (Fig. A.2).

The enhancement of mucoadhesion with the increase in HPC content in the formulation was as expected. HPC is used as a formulation component for tired eyes and in inserts for the dry eye syndrome, where it acts by stabilizing and thickening the tear film, prolonging tear film breakup time, lubricating and protecting the eye [66]. The source of HPC mucoadhesive properties lies in the formation of hydrogen bonds between its carboxylic acid group and glycoprotein of mucin proteins [26,67]. Mucoadhesive properties of the proposed DDS were strengthened and prolonged by the diffusion of polymers chains into the mucous membrane, which in turn was reinforced by high surface-area-to-volume ratio of the nanofibers [68]. The reason for the decrease of mucoadhesion potential in wet conditions, and lack of statistical differences between mucoadhesive properties of H7_BRZ in wet and H5_BRZ in dry conditions (Fig. 7), was the partial dissolution of HPC in the aqueous environment.

In comparison to the liquid carriers tested on corneal mucosa, the force of mucoadhesion of the best performance sample, H7cd_BRZ, was similar to the values reported in the literature, in some cases even exceeding them within the same order of magnitude [69,70]. The values of force and work of mucoadhesion of H7cd_BRZ were also in the range of those obtained for other nanofibrous drug carriers with the use of other mucin source, e.g. buccal tissue, except one case, where one order of magnitude higher work values were reached [71–73]. Most of the researchers did not include excessive wetting in the test methodology, therefore comparison involves the results obtained on dry corneas.

While there are numerous reports on nanofibers mucoadhesion to buccal, nasal or vaginal tissues, little attention is paid to ocular structures and ocular delivery based on adhesion [74]. To our best knowledge, this is the second report of a quantitative evaluation of mucoadhesive properties of nanofibers to fresh ocular mucosa using texture analyser [21].

3.8. Permeation of BRZ from nanofibers ex vivo

The drug permeation from all tested formulations was practically

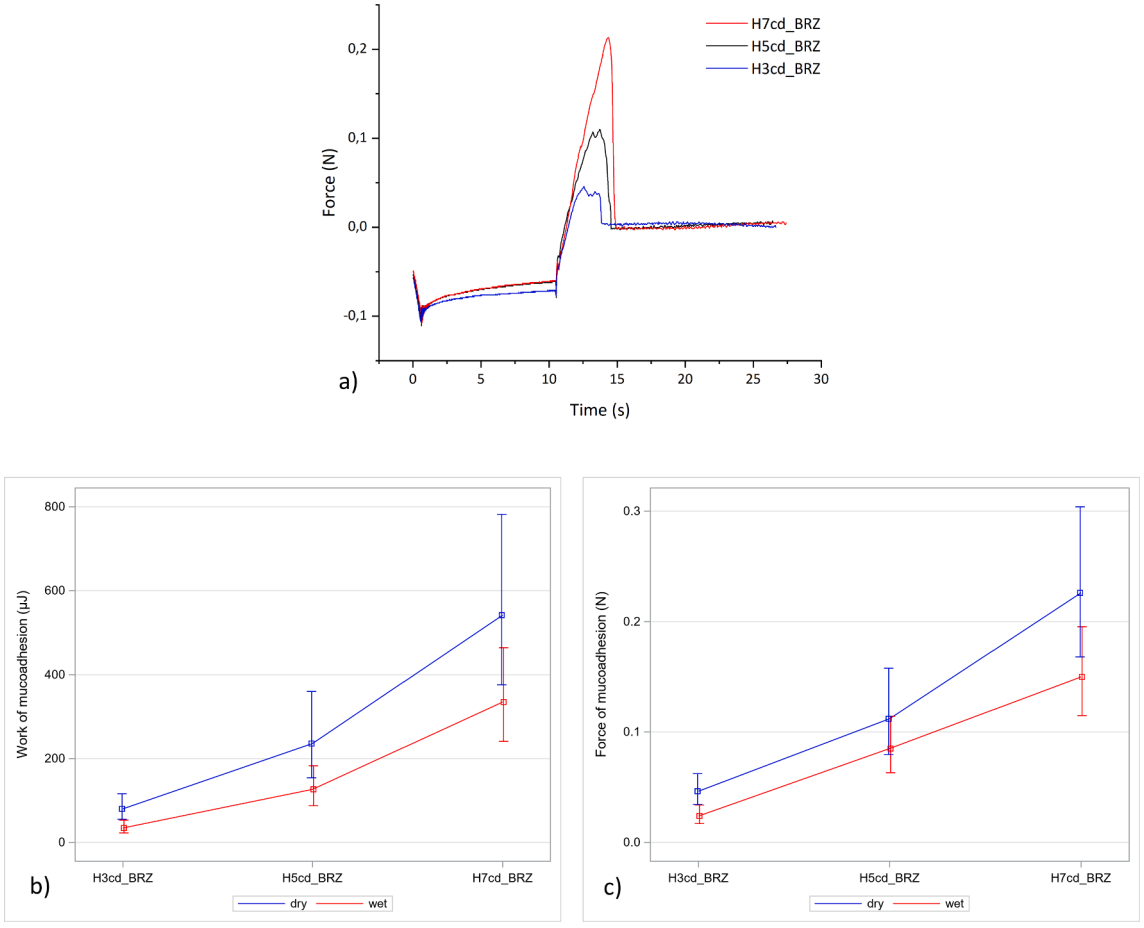

Fig. 7. Representative time vs force curves obtained during a mucoadhesion test (dry conditions) (a); average work (b) and force (c) of mucoadhesion of the BRZ-loaded nanofiber nonwovens. Data are expressed as a mean with 95% confidence limits (n = 4).

linear in time with very slightly higher rate at the beginning and occurred without burst release to the receptor medium. It did not start immediately, but after an initial lag phase, being a consequence of drug diffusion into the cornea before its release to the receiving solution as reported previously [75]. The permeation profiles of H5cd_BRZ, H7cd_BRZ and control Optilamid® were very similar and the amounts of permeated BRZ in each time point were statistically indifferent. Only H3cd_BRZ profile differed, as BRZ amounts in each time point, except after 60 min, were statistically higher, possibly due to PCL high permeability to small drug molecules [36]. Accordingly, steady state flux of H3cd_BRZ was statistically significantly higher than that of control, while fluxes of H7cd_BRZ and H5cd_BRZ were almost equally a little lower (Table 7). An average of 40.82, 41.2, 61.76 and 46.4 μg/cm^2 of BRZ permeated during 6 h from different nanofiber formulations, namely H7cd_BRZ, H5cd_BRZ, H3cd_BRZ and control Optilamid®, respectively (Fig. 8). Average delay in permeation was lower with the use of nanofiber nonwovens compared to the control (H5_BRZ < H3_BRZ < H7_BRZ), suggesting β-CD role in promoting drug partition into the corneal membrane, thus acting as a permeation enhancer in the initial phase. Considering data on steady state flux, this was particularly effective in sample H3cd_BRZ.

Obtained permeation profiles were similar to those reported in the literature for other BRZ carriers [11,12,14]. which accordingly exhibited similar BRZ permeation through corneas as their controls. *In vivo* evaluation of these carriers showed that the IOP achieved lower rates, yet the duration of this decrease was similar as obtained with controls. This points to the fact that improvement in drug solubility and corneal permeation should not be the final goal when optimizing ocular DDS, as key factors for prolonging the therapeutic potential are decreased clearance and localized delivery area. The developed nanofibrous BRZ carrier of our design meets all of the requirements – thanks to its mucoadhesiveness (Fig. 7) and BRZ/β-CD complex characteristics (Fig. 4), a reservoir of BRZ would be kept in the preocular space for a longer time, allowing the drug to permeate more effectively mostly through a tissue of preference, hence remain in the therapeutic window for much longer.

3.9. Cytotoxicity

In PrestoBlue assay, the viability of cells can be determined by measuring the fluorescence of coloured reagent as metabolically active cells are able to reduce the reagent and produce highly fluorescent molecule. Fluorescence values of the control (cells in growth medium) doubled approximately after each test day, confirming proper cell growth and therefore reliability of the test (Fig. 9). In case the growth medium was replaced with the nanofiber nonwoven extracts, cell growth and proliferation were also nicely observed in all time-points (up to 3 days), yet the fluorescence values were slightly lower than that of the corresponding controls. After one day of incubation in the extracts of BRZ-loaded materials, the activity of cells differed statistically between different formulations, decreasing in proportion to HPC content, and probably released BRZ (Fig. A.3). This was not evidenced the following days. Also, the activity of cells exposed to drug-loaded compared to non-loaded corresponding formulations was a little lower, yet the differences were statistically significant only between formulations H7 (all 3 days)

Table 7
Lag phase and steady state flux for the brinzolamide (BRZ)-loaded nanofibers and control; data of steady state flux are expressed with standard errors.

Formulation	Lag phase (min)	Steady state flux (Jss) (ug/cm^2/min)
H7cd_BRZ	38.48	0.1291 (+/-0.0096)
H5cd_BRZ	30.54	0.1264 (+/-0.0088)
H3cd_BRZ	33.76	0.1914 (+/-0.0106)
Optilamid®	57.53	0.1545 (+/-0.0101)

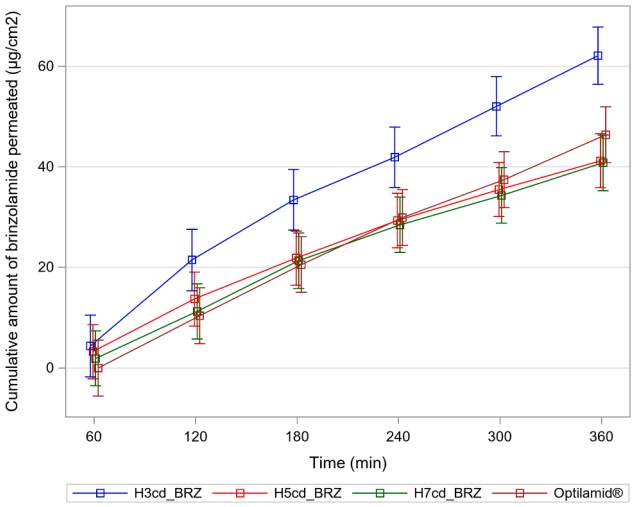

Fig. 8. Brinzolamide (BRZ) permeation through sheep corneas shown as absolute permeated amount of BRZ in time in mass per diffusion area (μg/cm^2). Data are expressed as a mean with 95% confidence limits (n = 16 for H7cd_BRZ and Optilamid®, n = 17 for H5cd_BRZ, n = 13 for H3cd_BRZ).

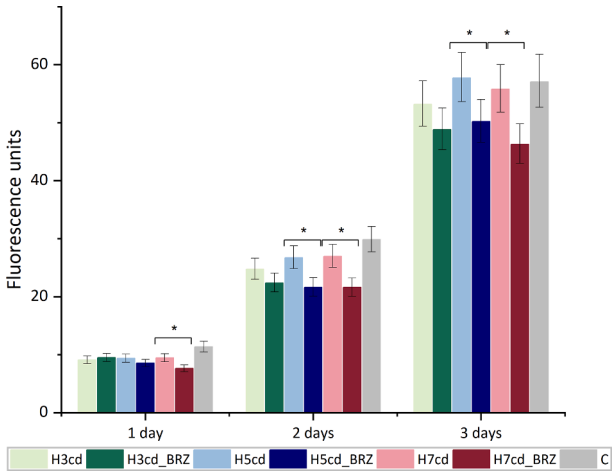

Fig. 9. Metabolic activity and viability of fibroblasts exposed to the extracts of nanofiber nonwovens (brinzolamide (BRZ)-loaded and non-loaded) for 1–3 days, shown as fluorescence units. Data are expressed as a mean with 95% confidence limits (n = 6). Statistically significant differences between corresponding formulations with and without the drug (H3cd_BRZ and H3cd; H5cd_BRZ and H5cd; H7cd_BRZ and H7cd) were marked as * ($p < 0.05$). Keys: C – cell control. Reference is made to Table 1 for different formulations.

and H5 (day 2 and 3, Fig. 9 and A.3). Interestingly, the comparison of fluorescence values to controls in separate days showed that the relative metabolic activity of the cells was the highest after three days of incubation in the extracts.

Indeed, the metabolic activity of cells was affected by the released HPC and BRZ in day 1, however, it was normalized after 3 days. This confirmed that the materials are not toxic to cells and do not release components that will irreversibly affect their viability. It is in accordance with expectations, as numerous evidences support the claims of biocompatibility of PCL, HPC is a pharmaceutical excipient, and BRZ concentration in commercial medications is comparable to the maximum concentrations achieved in the test wells.

3.10. Sterility of nanofiber nonwovens

Sterility testing was performed only for drug-free nanofiber

nonwovens, according to generally accepted methodology, to exclude the possible effect of the drug on bioburden reduction. UV is a first-choice sterilization method for nanofiber-based nonwovens in a laboratory scale and has been found appropriate to reduce the bioburden of many DDSs [76]. Time of the treatment was selected on the basis of literature reports of effective sterilization of 2D materials within 30 min or less per side [77].

The nanofiber nonwovens that were not subjected to UV treatment exhibited microbial growth shortly after initiating the test. UV treatment was found to be effective for decontaminating H5cd and H3cd nonwovens, as there was no microbial growth observed during 14 days in both aerobic and anaerobic conditions. Results for H7cd nonwoven were uncertain as one sample in FTG medium still exhibited microbial growth (Table 8). The controls were valid, as no microbial growth occurred in any of the negative controls, whereas in all positive controls the growth occurred.

Sterility is a critical quality attribute of implanted biomaterials, as infections due to bacterial contamination *in vivo* can result in severe complications [77]. In ocular applications, the risk is favored by bacterial entrapment under the implanted biomaterial, a phenomenon that was previously described for contact lenses [78]. Therefore, successful sterilization of the system brings it closer to real *in vivo* use.

3.11. Antibacterial activity

The controls were valid – erythromycin and tetracycline inhibited the growth of *S. aureus* and *P. aeruginosa* and their MIC amounted to 0.00025 mg/mL and 0.03125 mg/mL, respectively. No antibacterial activity of BRZ against *S. aureus* and *P. aeruginosa* was evidenced in the MIC test, and neither nanofibers did exhibit such activity. Due to the lack of arylamine moiety attached to a sulphonamide group in BRZ structure, assigning BRZ to the nonantibiotics group of sulfonamide drugs, the result is not surprising. The rationale for undertaking the study was BRZ's inhibitory potential against M. tuberculosis, and a similar CAI, dorzolamide, effectivity against vancomycin-resistant enterococci [79–81]. The choice of bacterial strains, *P. aeruginosa* and *S. aureus*, was also deliberate – they are commonly responsible for bacterial conjunctivitis, keratitis and endophthalmitis [82].

4. Summary and conclusions

In this research work, electrospun brinzolamide (BRZ)-loaded hydroxypropyl cellulose (HPC)/ polycaprolactone (PCL)/ β-cyclodextrin (β-CD) nanofibrous carriers intended for ocular application were designed, formed and systematically characterized. In the multicomponent materials, β-CD encapsulated poorly soluble BRZ within a solid nanofibrous structure, enabling its transport through an aqueous tear film to lipophilic corneal epithelium; HPC was responsible for mucoadhesive and eye-hydrating properties, and PCL – for the improvement of mechanical performance of the carriers. The synergistic action of all of the ingredients and the nanofibrous structure of the carriers was aimed at increasing the therapeutic potential in comparison with the traditional BRZ medications, by improving its delivery through cornea.

After the complex formation between BRZ and β-CD was confirmed in solutions and solid-state, proper morphology for BRZ-loaded nanofibers and reference materials were formed and subjected to several physicochemical tests. In the molecular structure study, interactions between BRZ and other components of the nanofibers were demonstrated, including β-CD/BRZ guest–host interactions. The drug was successfully incorporated and preserved in all drug-loaded nanofiber nonwovens during the electrospinning process. Compared to commercial formulation, developed nanofiber nonwoven formulation offered much more accurate dosing. It permeated through sheep corneas in a sustained manner, achieving therapeutic concentrations in the receptor medium. Increasing PCL ratio in the nonwovens led to the increase of a steady state flux, yet decreased adhesion to eye mucins *ex vivo*, which was relatively high for HPC-dominating materials. All formulations were found to be biocompatible, which was demonstrated by a high metabolic activity level of fibroblasts cultured in contact with material extracts in a modified cytotoxicity test. The mechanical properties of the nonwovens were also sufficient to handle them without special caution, and interesting differences in stress/strain curves were found related with the exact composition of the formulation. UV was found to be a proper method to reduce bioburden of the fibers' matrix, however, the carriers did not possess any anti-microbial properties.

With such characteristics, the BRZ-loaded HPC/PCL/β-CD nanofibrous carriers of our design, especially material H7cd_BRZ, offers a unique possibility of a significant extension of drug delivery primarily through a preferred tissue, cornea, to which it adheres, not affecting the already disturbed moisture of glaucomatous eyes. Developed formulation can be now directed towards *in vivo* tests on animals.

Table 8
Sterility of the non-drug-loaded nanofiber nonwovens after UV treatment: a number of samples exhibiting microbial growth out of three replicates. Reference is made to Table 1 for different formulations.

Sample	Untreated	30 min UV
H7cd in TSB	3/3	0/3
H7cd in FTG	1/3	1/3
H5cd in TSB	2/3	0/3
H5cd in FTG	2/3	0/3
H3cd in TSB	3/3	0/3
H3cd in FTG	3/3	0/3

Key: FTG – fluid thioglycollate medium, TSB – tryptic soy broth; UV- ultraviolet.

Declaration of Competing Interest

The authors declare that they have no known competing financial interests or personal relationships that could have appeared to influence the work reported in this paper.

Acknowledgements

This work was supported by the National Science Centre, Poland (grant number 2019/35/N/ST5/03882) and Estonian Research Council, Estonia (grant number PRG1507).

Appendix A. Supplementary material

Supplementary data to this article can be found online at https://doi.org/10.1016/j.ejpb.2022.09.008.

References

[1] D.-Y. Yu, S.J. Cringle, W.H. Morgan, Glaucoma Related Ocular Structure and Function, in: X, Sun, Y. Dai (Eds.), Medical Treatment of Glaucoma, Springer Nature Singapore Pte Ltd., Singapore, 2019, pp. 2, DOI: 10.1007/978-981-13-2733-9.
[2] N. Mahabadi, L.A. Foris, K. Tripathy, Open Angle Glaucoma. https://www.ncbi.nlm.nih.gov/books/NBK441887/#article-22264.s1 (accessed 2022-01-21).
[3] A.C. Momont, P.L. Kaufman, Medical Therapy for Glaucoma-IOP Lowering Agents, in: X, Sun, Y. Dai (Eds.), Medical Treatment of Glaucoma, Springer Nature Singapore Pte Ltd., Singapore, 2019, pp. 122-124, DOI: 10.1007/978-981-13-2733-9.
[4] B. Plazonnet, Ophthalmic drug delivery, in: M.J. Rathbone, J. Hadgraft, M.S. Roberts (Eds.), Modified-Release Drug Delivery Technology, Marcel Dekker, New York, USA, 2003, pp. 290-292, DOI: 10.1201/9780203910337.
[5] R. Jani, E. Rhone, Ion Exchange Resin Technology for Ophthalmic Applications, in: M.J. Rathbone, J. Hadgraft, M.S. Roberts (Eds.), Modified-Release Drug Delivery Technology, Marcel Dekker, New York, USA, 2003, p. 315, doi:10.1201/9780203910337.
[6] Y. Chen, K. Jiang, G. Wei, Y. Dai, Medical Treatment Strategy for Glaucoma, in: X, Sun, Y. Dai (Eds.), Medical Treatment of Glaucoma, Springer Nature Singapore Pte Ltd., Singapore, 2019, pp. 99-101, DOI: 10.1007/978-981-13-2733-9.
[7] E. Kanner, J.C. Tsai, Glaucoma medications: use and safety in the elderly population, Drugs & Aging 23 (4) (2006) 321–332.

[8] H.A. Salama, M. Ghorab, A.A. Mahmoud, M.A. Hady, PLGA nanoparticles as subconjunctival injection for management of glaucoma, AAPS PharmSciTech 18 (7) (2017) 2517–2528, https://doi.org/10.1208/s12249-017-0710-8.
[9] M.V. Fedorchak, I.P. Conner, C.A. Medina, J.B. Wingard, J.S. Schuman, S.R. Little, 28-day intraocular pressure reduction with a single dose of brimonidine tartrate-loaded microspheres, Exp. Eye Res. 125 (2014) 210–216, https://doi.org/10.1016/j.exer.2014.06.013.
[10] R. Tailor, R. Beasley, Y. Yang, N. Narendran, Evaluation of patients' experiences at different stages of the intravitreal injection procedure – what can be improved? Clin. Ophthalmol. 5 (2011) 1499–1502, https://doi.org/10.2147/OPTH.S24358.
[11] W. Wu, J. Li, L. Wu, B. Wang, Z. Wang, Q. Xu, H. Xin, Ophthalmic delivery of brinzolamide by liquid crystalline nanoparticles, in vitro and in vivo evaluation, AAPS PharmSciTech 14 (3) (2013) 1063–1071, https://doi.org/10.1208/s12249-013-9997-2.
[12] F. Wang, X. Bao, A. Fang, H. Li, Y. Zhou, Y. Liu, C. Jiang, J. Wu, X. Song, Nanoliposome-encapsulated brinzolamide-hydropropyl-β-cyclodextrin Inclusion complex: a potential therapeutic ocular drug-delivery system, Front. Pharmacol. 9 (91) (2018), https://doi.org/10.3389/fphar.2018.00091.
[13] H. Bhalerao, K.B. Koteshwara, S. Chandran, Design, optimisation and evaluation of in situ gelling nanoemulsion formulations of brinzolamide, Drug Delivery Transl. Res. 10 (2020) 529–547, https://doi.org/10.1007/s13346-019-00697-0.
[14] V. Dubey, P. Mohan, J.S. Dangi, K. Kesavan, Brinzolamide loaded chitosan-pectin mucoadhesive nanocapsules for management of glaucoma: Formulation, characterization and pharmacodynamic study, Int. J. Biol. Macromol. 152 (2020) 1224–1232, https://doi.org/10.1016/j.ijbiomac.2019.10.219.
[15] A. Peral, A. Martinez-Aguila, C. Pastrana, F. Huete-Toral, C. Carpena-Torres, G. Carracedo, Contact lenses as drug delivery system for glaucoma: a review, Appl. Sci. 10 (15) (2020) 5151, https://doi.org/10.3390/app10155151.
[16] J.R. Franca, G. Foureaux, L.L. Fuscaldi, T.G. Ribeiro, L.B. Rodrigues, R. Bravo, R. O. Castilho, M.I. Yoshida, V.B. Cardoso, S.O. Fernandes, S. Cronemberger, A. J. Ferreira, A.A.G. Faraco, Bimatoprost-loaded ocular inserts as sustained release drug delivery systems for glaucoma treatment. In vitro and in vivo evaluation, PLOS ONE 9 (4) (2014), https://doi.org/10.1371/journal.pone.0095461.g002.
[17] P. Bhagav, V. Trivedi, D. Shah, S. Chandran, Sustained release ocular inserts of brimonidine tartrate for better treatment in open-angle glaucoma, Drug Delivery Transl. Res. 1 (2011) 161–174, https://doi.org/10.1007/s13346-011-0018-2.
[18] C.C. Peng, M.T. Burke, B.E. Carbia, C. Plummer, A. Chauhan, Extended drug delivery by contact lenses for glaucoma therapy, J. Controlled Release 162 (2012) 152–158, https://doi.org/10.1016/j.jconrel.2012.06.017.
[19] J.B. Ciolino, C.F. Stefanescu, A.E. Ross, B. Salvador-Culla, P. Cortez, E.M. Ford, K. A. Wymbs, S.L. Sprague, D.R. Mascoop, S.S. Rudina, S.A. Trauger, F. Cade, D. S. Kohane, In vivo performance of a drug-eluting contact lens to treat glaucoma, Biomaterials 35 (2014) 432–439, https://doi.org/10.1016/j.biomaterials.2013.09.032.
[20] C. Karavasili, A. Komnenou, O.L. Katsamenis, G. Charalampidou, E. Kofidou, D. Andreadis, S. Koutsopoulos, D.G. Fatouros, Self-assembling peptide nanofiber hydrogels for controlled ocular delivery of timolol maleate, ACS Biomater. Sci. Eng. 3 (12) (2017) 3386–3394, https://doi.org/10.1021/acsbiomaterials.7b00706.
[21] Gagandeep, T. Garg, B. Malik, G. Rath, A.K. Goyal, Goyal, Development and characterization of nano-fiber patch for the treatment of glaucoma, Eur. J. Pharm. Sci. 53 (2014) 10–16.
[22] S.K. Yellanki, B. Anna, M.R. Kishan, Preparation and in vivo evaluation of sodium alginate - poly (vinyl alcohol) electrospun nanofibers of forskolin for glaucoma treatment, Pak. J. Pharm. Sci. 32 (2) (2019) 669–674.
[23] S. Omer, R. Zelkó, A systematic review of drug-loaded electrospun nanofiber-based ophthalmic inserts, Pharmaceutics 13 (2021) 1637, https://doi.org/10.3390/pharmaceutics13101637.
[24] A. Luraghi, F. Peri, L. Moroni, Electrospinning for drug delivery applications: a review, J. Controlled Release 334 (2021) 463–484, https://doi.org/10.1016/j.jconrel.2021.03.033.
[25] B. Göttel, J.M. de Souza e Silva, C. Santos de Oliveira, F. Syrowatka, M. Fiorentzis, A. Viestenz, A. Viestenz, K. Mäder, Electrospun nanofibers – a promising solid in-situ gelling alternative for ocular drug delivery, Eur. J. Pharm. Biopharm. 146 (2020) 125–132.
[26] A. Sosnik, J. das Neves, B. Sarmento, Mucoadhesive polymers in the design of nano-drug delivery systems for administration by non-parenteral routes: a review, Prog. Polym. Sci. 39 (12) (2014) 2030–2075.
[27] J. Xue, T. Wu, Y. Dai, Y. Xia, Electrospinning and electrospun nanofibers: methods, materials, and applications, Chem. Rev. 119 (8) (2019) 5298–5415, https://doi.org/10.1021/acs.chemrev.8b00593.
[28] P. Jansook, H.M. Hnin, T. Loftsson, E. Stefánsson, Cyclodextrin-based formulation of carbonic anhydrase inhibitors for ocular delivery – a review, Int. J. Pharm. 606 (2021) 120955.
[29] M. Schmitt, Design and Development of Ocular Formulations for Preclinical and Clinical Trials, in: Y. Bachhav (Ed.), Innovative Dosage Forms: Design and Development at Early Stage, Wiley-VCH Verlag GmbH & Co., KGaA, Germany, 2019, pp. 331–365, https://doi.org/10.1002/9783527812172.ch10.
[30] T. Kida, S. Sato, H. Yoshida, A. Teragaki, M. Akashi, 1,1,1,3,3,3-Hexafluoro-2-propanol (HFIP) as a novel and effective solvent to facilely prepare cyclodextrin-assembled materials, ChemComm 50 (2014) 14245–14248, https://doi.org/10.1039/c4cc06690a.
[31] A. Costoya, A. Concheiro, C. Alvarez-Lorenzo, Electrospun fibers of cyclodextrins and poly(cyclodextrins), Molecules 22 (2) (2017) 230.
[32] S. Kamel, N. Ali, K. Jahangir, S.M. Shah, A.A. El-Gendy, Pharmaceutical significance of cellulose: a review, Express Polym. Lett. 2 (11) (2008) 758–778.
[33] L.M. Gradinaru, M. Barbalata-Mandru, M. Drobota, M. Aflori, M. Spiridon, G. G. Pircalabioru, C. Bleotu, M. Butnaru, S. Vlad, Preparation and evaluation of nanofibrous hydroxypropyl cellulose and β-cyclodextrin polyurethane composite mats, Nanomaterials 10 (4) (2020), https://doi.org/10.3390/nano10040754.
[34] M.H. El-Newehy, M.E. El-Naggar, S. Alotaiby, H. El-Hamshary, M. Moydeen, S. Al-Deyab, Green electrospining of hydroxypropyl cellulose nanofibres for drug delivery applications, J Nanosci Nanotechnol 18 (2) (2018) 805–814, https://doi.org/10.1166/jnn.2018.13852.
[35] N. Chinatangkul, S. Pengon, S. Piriyaprasarth, C. Limmatvapirat, A. Limmatvapirat, Development of electrospun shellac and hydroxypropyl cellulose blended nanofibers for drug carrier application, Key Eng. Mater. 859 (2020) 239–243, https://doi.org/10.4028/www.scientific.net/KEM.859.239.
[36] M.A. Woodruff, D.W. Hutmacher, The return of a forgotten polymer—Polycaprolactone in the 21st century, Prog. Polym. Sci. 35 (2010) 1217–1256, https://doi.org/10.1016/j.progpolymsci.2010.04.002.
[37] P. Denis, J. Dulnik, P. Sajkiewicz, Electrospinning and structure of bicomponent polycaprolactone/gelatin nanofibers obtained using alternative solvent system, Int. J. Polym. Mater. Polym. Biomater. 64 (7) (2015) 354–364, https://doi.org/10.1080/00914037.2014.945208.
[38] K.A.G. Katsogiannis, G.T. Vladisavljevic, S. Georgiadou, Porous electrospun polycaprolactone (PCL) fibres by phase separation, Eur. Polym. J. 69 (2015) 284–295, https://doi.org/10.1016/j.eurpolymj.2015.01.028.
[39] T. Loftsson, P. Jarho, M. Másson, T. Järvinen, Cyclodextrins in drug delivery (Review), Expert Opin. Drug Delivery 2 (2) (2005) 335–351, https://doi.org/10.1517/17425247.2.1.335.
[40] C.A. Greene, S.L. Misra, H. Lee, J. McKelvie, K. Kapadia, R. McFarlane, C.N. J. McGhee, C.R. Green, T. Sherwin, The sheep cornea: structural and clinical characteristics, Current Eye Research 43 (12) (2018) 1432–1438.
[41] N. García-Porta, F.J. Gantes-Nuñez, J. Tabernero, S. Pardhan, Characterization of the ocular surface temperature dynamics in glaucoma subjects using long-wave infrared thermal imaging, J. Opt. Soc. Am. A 36 (2019) 1015–1021, https://doi.org/10.1364/JOSAA.36.001015.
[42] CLSI. Performance Standards for Antimicrobial Susceptibility Testing; Twenty-Eight Informational Supplement (M100-S28); Clinical and Laboratory Standards Institute: Wayne, PA, USA or ISO 20776-1:2019.
[43] A. Vo, X. Feng, D. Patel, A. Mohammad, M. Patel, J. Zheng, D. Kozak, S. Choi, M. Ashraf, X. Xu, In vitro physicochemical characterization and dissolution of brinzolamide ophthalmic suspensions with similar composition, Int. J. Pharm. 588 (2020) 119761.
[44] H. Rachmawati, C.A. Edityaningrum, R. Mauludin, Molecular inclusion complex of curcumin-β-cyclodextrin nanoparticle to enhance curcumin skin permeability from hydrophilic matrix gel, AAPS PharmSciTech 14 (4) (2013) 1303–1312, https://doi.org/10.1208/s12249-013-0023-5.
[45] M.A. Medeleanu, D.I. Hădărugă, C.V. Muntean, G. Popescu, M. Rada, A. Hegheș, S. E. Zippenfening, C.A. Lucan (Banciu), A.B. Velciov, G.N. Bandur, N.G. Hădărugă, M. Riviș, Structure-property relationships on recrystallized β-cyclodextrin solvates: a focus on X-ray diffractometry, FTIR and thermal analyses, Carbohydr. Polym. 265 (2021) 118079.
[46] B. Czarnik-Matusewicz, S. Pilorz, L.-P. Zhang, Y. Wu, Structure of hexafluoroisopropanol–water mixture studied by FTIR-ATR spectra and selected chemometric methods, J. Mol. Struct. 883–884 (2008) 195–202, https://doi.org/10.1016/j.molstruc.2007.11.062.
[47] C. Shan, C. Ning, J. Lou, W. Xu, Y. Zhang, Design and preparation of UV-curable waterborne polyurethane based on novel fuorinated chain extender, Polym. Bull. 78 (2021) 2067–2083, https://doi.org/10.1007/s00289-020-03202-7.
[48] V. Crupi, D. Majolino, V. Venuti, G. Guella, I. Mancini, B. Rossi, P. Verrocchio, G. Viliani, R. Stancanelli, Temperature effect on the vibrational dynamics of cyclodextrin inclusion complexes: investigation by FTIR-ATR spectroscopy and numerical simulation, J. Phys. Chem. A 114 (2010) 6811–6817, https://doi.org/10.1021/jp101888g.
[49] N. Li, J. Liu, X. Zhao, Y. Gao, L. Zheng, J. Zhang, L. Yu, Complex formation of ionic liquid surfactant and β-cyclodextrin, Colloids Surf. A: Physicochem. Eng. Asp. 292 (2–3) (2007) 196–201, https://doi.org/10.1016/j.colsurfa.2006.06.023.
[50] E. Fenyvesi, L. Szente, Nanoencapsulation of flavors and aromas by cyclodextrins, in: A.M. Grumezescu (Ed.), Encapsulations. Nanotechnology in the Agri-Food Industry, Academic Press, 2016, pp. 769–792, https://doi.org/10.1016/C2015-0-01029-2.
[51] M.E. Brewster, T. Loftsson, Cyclodextrins as pharmaceutical solubilizers, Adv. Drug Delivery Rev. 59 (7) (2007) 645–666.
[52] P. Jansook, E. Stefánsson, M. Thorsteinsdóttir, B.B. Sigurdsson, S.S. Kristjánsdóttir, J.F. Bas, H.H. Sigurdsson, T. Loftsson, Cyclodextrin solubilization of carbonic anhydrase inhibitor drugs: formulation of dorzolamide eye drop microparticle suspension, Eur. J. Pharm. Biopharm. 76 (2010) 208–214, https://doi.org/10.1016/j.ejpb.2010.07.005.
[53] D. Lockington, E.C.A. Macdonald, P. Stewart, D. Young, M. Caslake, K. Ramaesh, Free radicals and the pH of topical glaucoma medications: a lifetime of ocular chemical injury? Eye 26 (2012) 734–741, https://doi.org/10.1038/eye.2012.25.
[54] Á. Haimhoffer, Á. Rusznyák, K. Réti-Nagy, G. Vasvári, J. Váradi, M. Vecsernyés, I. Bácskay, P. Fehér, Z. Ujhelyi, F. Fenyvesi, Cyclodextrins in drug delivery systems and their effects on biological barriers, Sci. Pharm. 87 (4) (2019) 33.
[55] T. Loftsson, P. Jansook, E. Stefansson, Topical drug delivery to the eye: Dorzolamide, Acta Ophthalmol. 90 (2012) 603–608, https://doi.org/10.1111/j.1755-3768.2011.02299.x.
[56] S. Ali, Z. Khatri, K.W. Oh, I.-S. Kim, S.H. Kim, Preparation and characterization of hybrid polycaprolactone/cellulose ultrafine fibers via electrospinning, Macromol. Res. 22 (5) (2014) 562–568, https://doi.org/10.1007/s13233-014-2078-x.

[57] K. Phillipson, M.J. Jenkins, J.N. Hay, The kinetics of crystallization of poly (ε-caprolactone) measured by FTIR spectroscopy, J. Therm. Anal. Calorim. 123 (2016) 1491–1500, https://doi.org/10.1007/s10973-015-5047-5 63.
[58] N.D. Alharbi, O.W. Guirguis, Macrostructure and optical studies of hydroxypropyl cellulose in pure and Nano-composites forms, Results Phys. 15 (2019) 102637.
[59] J.K. Jethava, G.K. Jethava, Design, formulation, and evaluation of novel sustain release bioadhesive in-situ gelling ocular inserts of ketorolac tromethamine, Int. J. Pharm. Invest. 4 (4) (2014) 226–232, https://doi.org/10.4103/2230-973X.143131.
[60] S. Mehrandish, G. Mohammadi, S. Mirzaeei, Preparation and functional evaluation of electrospun polymeric nanofibers as a new system for sustained topical ocular delivery of itraconazole, Pharm. Dev. Technol. 27 (1) (2022) 25–39, https://doi.org/10.1080/10837450.2021.2018609.
[61] H. Abdelkader, D. Wertheim, B. Pierscionek, R.G. Alany, Curcumin in situ gelling polymeric insert with enhanced ocular performance, Pharmaceutics 12 (12) (2020) 1158, https://doi.org/10.3390/pharmaceutics12121158.
[62] M. Tighsazzadeh, J.C. Mitchell, J.S. Boateng, Development and evaluation of performance characteristics of timolol-loaded composite ocular films as potential delivery platforms for treatment of glaucoma, Int. J. Pharm. 566 (2019) 111–125, https://doi.org/10.1016/j.ijpharm.2019.05.059.
[63] R. Kalyanwat, B. Shrivastava, K. Pathak, Preparation and Evaluation of bioadhesive ocular inserts of aceclofenac, Int. J. Pharm. Sci. Rev. Res. 41 (2) (2016) 207–213.
[64] S. Singamaneni, S. Chang, J.-H. Jang, W. Davis, E.L. Thomas, V.V. Tsukruk, Mechanical properties of composite polymer microstructures fabricated by interference lithography, Phys. Chem. Chem. Phys. 10 (2008) 4093–4105, https://doi.org/10.1039/b719709h.
[65] E. Zussman, D. Rittel, A.L. Yarin, Failure modes of electrospun nanofibers, Appl. Phys. Lett. 82 (22) (2003) 3958–3960.
[66] T. Nguyen, R. Latkany, Review of hydroxypropyl cellulose ophthalmic inserts for treatment of dry eye, Clin. Ophthalmol. 5 (2011) 587–591, https://doi.org/10.2147/OPTH.S13889.
[67] B. Chatterjee, N. Amalina, P. Sengupta, U.K. Mandal, Mucoadhesive polymers and their mode of action: a recent update, J. Appl. Pharm. Sci. 7 (05) (2017) 195–203, https://doi.org/10.7324/JAPS.2017.70533.
[68] R.S. Dave, T.C. Goostrey, M. Ziolkowska, S. Czerny-Holownia, T. Hoare, H. Sheardown, Ocular drug delivery to the anterior segment using nanocarriers: a mucoadhesive/mucopenetrative perspective, J. Controlled Release 336 (2021) 71–88, https://doi.org/10.1016/j.jconrel.2021.06.011.
[69] S. Akhter, M. Anwar, M.A. Siddiqui, I. Ahmad, J. Ahmad, M.Z. Ahmad, A. Bhatnagar, F.J. Ahmad, Improving the topical ocular pharmacokinetics of animmunosuppressant agent with mucoadhesive nanoemulsions: Formulation development, in vitro and in vivo studies, Colloids Surf. B: Biointerfaces 148 (2016) 19–29, https://doi.org/10.1016/j.colsurfb.2016.08.048.
[70] B. Lorenzo-Veiga, P. Diaz-Rodriguez, C. Alvarez-Lorenzo, T. Loftsson, H. H. Sigurdsson, In vitro and ex vivo evaluation of nepafenac-based cyclodextrin microparticles for treatment of eye inflammation, Nanomaterials 10 (4) (2020), https://doi.org/10.3390/nano10040709.
[71] M.B. Stie, J.R. Gätke, F. Wan, I.S. Chronakis, J. Jacobsen, H.M. Nielsen, Swelling of mucoadhesive electrospun chitosan/polyethylene oxide nanofibers facilitates adhesion to the sublingual mucosa, Carbohydr. Polym. 242 (2020) 116428.
[72] C. Dott, C. Tyagi, L.K. Tomar, Y.E. Choonara, P. Kumar, L.C. du Toit, V. Pillay, A mucoadhesive electrospun nanofibrous matrix for rapid oramucosal drug delivery, J. Nanomater. 2013 (2013) 1–19, https://doi.org/10.1155/2013/924947.
[73] F. Brako, R. Thorogate, S. Mahalingam, B. Raimi-Abraham, D.Q.M. Craig, M. Edirisinghe, Mucoadhesion of progesterone-loaded drug delivery nanofiber constructs, ACS Appl. Mater. Interfaces 10 (2010) 13381–13389, https://doi.org/10.1021/acsami.8b03329.
[74] G.L. Pérez-González, L.J. Villarreal-Gómez, A. Serrano-Medina, E.J. Torres-Martínez, J.M. Cornejo-Bravo, Mucoadhesive electrospun nanofibers for drug delivery systems: applications of polymers and the parameters' roles, Int. J. Nanomed. 14 (2019) 5271–5285, https://doi.org/10.2147/IJN.S193328.
[75] I. Rodriguez, J.A. Vázquez, L. Pastrana, V.V. Khutoryanskiy, Enhancement and inhibition effects on the corneal permeability of timolol maleate: polymers, cyclodextrins and chelating agents, Int. J. Pharm. 529 (1–2) (2017) 168–177, https://doi.org/10.1016/j.ijpharm.2017.06.075.
[76] C.F. Rediguieri, R.C. Sassonia, K. Dua, I.S. Kikuchi, T.J.A. Pinto, Impact of sterilization methods on electrospun scaffolds for tissue engineering, Eur. Polym. J. 82 (2016) 181–195, https://doi.org/10.1016/j.eurpolymj.2016.07.016.
[77] L. Preem, E. Vaarmets, A. Meos, I. Jõgi, M. Putriņš, T. Tenson, K. Kogermann, Effects and efficacy of different sterilization and disinfection methods on electrospun drug delivery systems, Int. J. Pharm. 567 (2019), 118450, https://doi.org/10.1016/j.ijpharm.2019.118450.
[78] S.M.J. Fleiszig, A.R. Kroken, V. Nieto, M.R. Grosser, S.J. Wan, M.M.E. Metruccio, D.J. Evans, Contact lens-related corneal infection: intrinsic resistance and its compromise, Prog. Retinal Eye Res. 76 (2020) 100804.
[79] T.E. Kelly, P.H. Hackett, Acetazolamide and sulfonamide allergy: a not so simple story, High Alt. Med. Biol. 11 (4) (2010) 319–323, https://doi.org/10.1089/ham.2010.1051.
[80] I. Nishimori, T. Minakuchi, D. Vullo, A. Scozzafava, A. Innocenti, C.T. Supuran, Carbonic anhydrase inhibitors. Cloning, characterization, and inhibition studies of a new β-carbonic anhydrase from mycobacterium tuberculosis, J. Med. Chem. 52 (9) (2009) 3116–3120.
[81] N.S. Abutaleb, A.E.M. Elhassanny, D.P. Flaherty, M.N. Seleem, In vitro and in vivo activities of the carbonic anhydrase inhibitor, dorzolamide, against vancomycin-resistant enterococci, PeerJ 9 (2021), e11059, https://doi.org/10.7717/peerj.11059.
[82] S. Watson, M. Cabrera-Aguas, P. Khoo, Common eye infections, Aust. Prescr. 41 (3) (2018), https://doi.org/10.18773/austprescr.2018.016.